p-NO2-Bn-H(4)neunpa and H(4)neunpa-Trastuzumab

Spreckelrneyer, Sarah; Ramogida, Caterina F.; Rousseau, Julie; Arane, Karen; Bratanovic, Ivica; Colpo, Nadine; Jermilova, Una; Dias, Gernma M.; Dude, Julia; Jaraquemada-Pelaez, Maria de Guadalupe

Published in:
BIOCONJUGATE CHEMISTRY

DOI:
10.1021/acs.bioconjchem.7b00311

Publication date:
2017

Bioconjugate Chemistry

Article

pubs.acs.org/bc

p-NO_2−Bn−H_4neunpa and H_4neunpa−Trastuzumab: Bifunctional Chelator for Radiometalpharmaceuticals and ^{111}In Immuno-Single Photon Emission Computed Tomography Imaging

Sarah Spreckelmeyer,[†,‡] Caterina F. Ramogida,[§] Julie Rousseau,[∥] Karen Arane,[†] Ivica Bratanovic,[§] Nadine Colpo,[∥] Una Jermilova,[§] Gemma M. Dias,[∥] Iulia Dude,[∥] Maria de Guadalupe Jaraquemada-Peláez,[†] François Bénard,[∥] Paul Schaffer,[§] and Chris Orvig*[,†]

[†]Medicinal Inorganic Chemistry Group, Department of Chemistry, University of British Columbia, 2036 Main Mall, Vancouver, British Columbia V6T 1Z1, Canada

[‡]Department of Pharmacokinetics, Toxicology and Targeting, Research Institute of Pharmacy, University of Groningen, Antonius Deusinglaan 1, Groningen 9713 AV, The Netherlands

[§]Life Sciences Division, TRIUMF, 4004 Wesbrook Mall, Vancouver, British Columbia V6T 2A3, Canada

[∥]BC Cancer Agency, 675 West 10th Avenue, Vancouver, British Columbia V5Z 1L3, Canada

Supporting Information

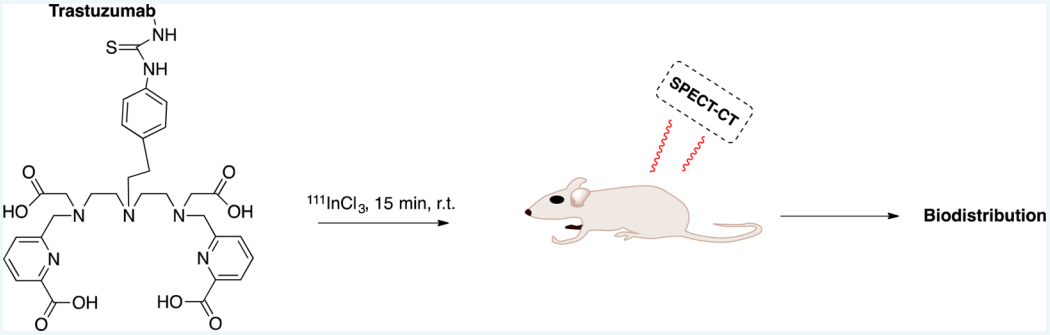

ABSTRACT: Potentially nonadentate (N_5O_4) bifunctional chelator *p*-SCN−Bn−H_4neunpa and its immunoconjugate H_4neunpa−trastuzumab for ^{111}In radiolabeling are synthesized. The ability of *p*-SCN−Bn−H_4neunpa and H_4neunpa−trastuzumab to quantitatively radiolabel $^{111}InCl_3$ at an ambient temperature within 15 or 30 min, respectively, is presented. Thermodynamic stability determination with In^{3+}, Bi^{3+}, and La^{3+} resulted in high conditional stability constant (*p*M) values. In vitro human serum stability assays have demonstrated both ^{111}In complexes to have high stability over 5 days. Mouse biodistribution of $[^{111}In][In(p\text{-}NO_2\text{−}Bn\text{−}neunpa)]^-$, compared to that of $[^{111}In][In(p\text{-}NH_2\text{−}Bn\text{−}CHX\text{-}A''\text{−}diethylenetriamine pentaacetic acid (DTPA))]^{2-}$, at 1, 4, and 24 h shows fast clearance of both complexes from the mice within 24 h. In a second mouse biodistribution study, the immunoconjugates ^{111}In-neunpa−trastuzumab and ^{111}In−CHX-A″−DTPA−trastuzumab demonstrate a similar distribution profile but with slightly lower tumor uptake of ^{111}In-neunpa−trastuzumab compared to that of ^{111}In−CHX-A″−DTPA−trastuzumab. These results were also confirmed by immuno-single photon emission computed tomography (immuno-SPECT) imaging in vivo. These initial investigations reveal the acyclic bifunctional chelator *p*-SCN−Bn−H_4neunpa to be a promising chelator for ^{111}In (and other radiometals) with high in vitro stability and also show H_4neunpa−trastuzumab to be an excellent ^{111}In chelator with promising biodistribution in mice.

INTRODUCTION

Early detection and specific therapy are the key factors for the successful treatment of cancer. ^{111}In ($t_{1/2}$ = 2.8 days) and/or ^{177}Lu ($t_{1/2}$ = 6.6 days) are important radioisotopes in nuclear medicine that match either the requirements for single photon emission tomography (SPECT) and performing dosimetry or for therapeutic purposes, respectively.[1139] ^{111}In, being a cyclotron-produced radiometal (via the ^{111}Cd(p,n)^{111}In reaction), emits γ rays (245 and 171 keV) and Auger electrons. ^{177}Lu, being a reactor-produced radiometal (^{176}Lu(n,γ)^{177}Lu), emits primarily β particles (490 keV) that can be used for therapy.[1]

A common method to incorporate metallic radioisotopes (i.e., radiometals) into radiopharmaceuticals is via chelation of the desired radioisotope using a bifunctional chelator (BFC). As implied by the name, BFCs possess two properties: they

Received: June 5, 2017
Revised: July 3, 2017
Published: July 6, 2017

DOI: 10.1021/acs.bioconjchem.7b00311
Bioconjugate Chem. 2017, 28, 2145−2159

must chelate the radiometal of interest in a tight and stable metal−ligand complex, and the BFC must incorporate a point of attachment for conjugation to a targeting vector (e.g., the biomolecule of interest in disease progression such as a peptide or antibody). Both macrocyclic and acyclic chelators are used in the clinic and are also of interest in the field of medicinal inorganic chemistry research. The pros and cons of cyclic versus acyclic chelators are widely known and beyond debate.[2] Relevant to ^{111}In and ^{177}Lu, macrocyclic 1,4,7,10-tetraazacyclododecane-1,4,7,10-tetraacetic acid (DOTA) is the gold-standard chelator, while acyclic chelator diethylenetriamine pentaacetic acid (DTPA) and chiral analogue CHX-A″−DTPA are ubiquitous in ^{111}In radiopharmaceutical development (Figure 1). Recent studies developed bifunctional somatostatin

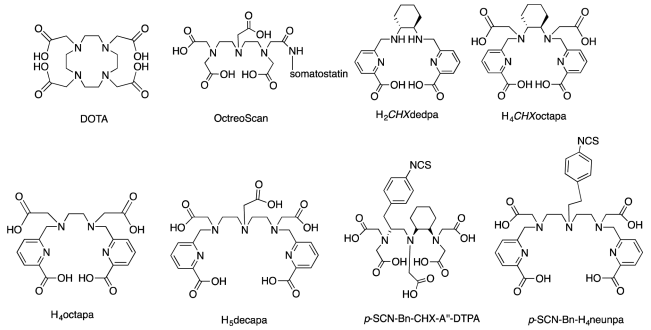

Figure 1. Structures of cyclic (DOTA) and acyclic (OctreoScan, CHX−A″-DTPA) commercial chelators, and acyclic "pa" ligands H_2CHXdedpa, H_4CHXoctapa, H_4octapa, H_5decapa, and novel nonadentate chelator *p*-SCN−Bn−H_4neunpa discussed in this work.

analogues of DOTA with increased stability in vivo.[3] As an acyclic gold standard, the commercially available radiopharmaceutical OctreoScan (^{111}In−DTPA octeotride) reached approval in 1994 (Figure 1). Since the success of OctreoScan, several more bifunctional acyclic ^{111}In chelators that contain different biomolecules have been developed, hoping to overcome the limitations of OctreoScan. These include an increased physiological uptake, which restricts the detection of small lesions, prolonged imaging protocol, and relatively high radiation doses to the patients as well as low image quality.[4]

Our group has developed several promising acyclic chelators for ^{111}In and ^{177}Lu based on picolinic acid binding motifs, which we have since dubbed the "pa" family of chelators.[5−8] Of note is the fact that octadentate H_4octapa (N_4O_4) and its bifunctional analogue *p*-SCN−Bn−H_4octapa showed exceptional complexation properties (quantitative ^{111}In or ^{177}Lu radiolabeling in 10−30 min at ambient temperature) and favorable in vivo stability of resulting complexes.[9,10] Furthermore, chiral ligands H_2*CHX*dedpa (N_4O_2) and H_4*CHX*octapa (N_4O_4) showed promising ^{68}Ga and ^{111}In radiolabeling properties, respectively, and subsequently impressive stability in human serum.[8]

Our group continues to design ligands that may incorporate large metal ions (such as radioactive actinides and lanthanides for imaging and therapy), which possess ideal properties for radiopharmaceutical incorporation, e.g. fast, mild, and quantitative complexation of radiometals at low ligand concentrations; formation of resultant thermodynamically stable and kinetically inert metal complexes; and a convenient point of attachment to targeting vectors. Herein, we report the synthesis and characterization of a novel nonadentate (CN = 9) acyclic chelator H_4neunpa (N_5O_4, referred to herein as either *p*-NO_2−Bn−H_4neunpa or H_4neunpa) and bifunctional analogue *p*-SCN−Bn−H_4neunpa that was designed as a bifunctional analogue of H_5decapa (N_5O_5), reported by our group in 2012.[5] The carboxylic acid group on the middle nitrogen atom has been replaced by *p*-nitrobenzene−ethylene to keep its symmetry and act as the bifunctional arm to attach the ligand to a biomolecule through a thiourea bond (Figure 1). We hypothesized that the extended diethylenetriamine backbone and nine coordinating atoms of H_4neunpa may favorably form complexes with large metal ions such as In^{3+} (92 pm, CN = 8),[11] Lu^{3+} (103 pm, CN = 9), or Bi^{3+} (117 pm, CN = 8). The radiolabeling of ^{111}In and ^{177}Lu to H_4neunpa was assessed and compared to gold standards DOTA and CHX-A″−DTPA, and an in vivo biodistribution study of H_4neunpa and CHX-A″−DTPA labeled with ^{111}In was performed. Thermodynamic stability constants of selected metal−neunpa complexes were also determined. Moreover, coupling of the HER2/*neu*-targeting monoclonal antibody (mAb) trastuzumab was performed via the reaction between the antibody's primary amine(s) with the isothiocyanate functional group of *p*-SCN−Bn−H_4neunpa. The bioconjugate was labeled with ^{111}In, and in vivo biodistribution, and single photon emission computed tomography−computed tomography (SPECT-CT) imaging studies were conducted and compared directly to a ^{111}In−CHX-A″−DTPA−trastuzumab conjugate.

RESULTS AND DISCUSSION

Synthesis and Characterization of the Ligand. The synthesis of the previously reported analogue H_5decapa used *N*-benzyl protection, *N*-alkylation with an alkyl halide, benzyl deprotection via hydrogenation, a second alkyl halide *N*-alkylation, and, finally, deprotection in refluxing HCl (6M).[10] The *N*-benzyl protection was found to be the yield-limiting step because the deprotection always resulted in partly elimination of the picolinic acid moieties. The use of *O*-nitrobenzenesulfonyl (nosyl) was found to give better cumulative yields compared to *N*-benzyl protection. Based on that, the bifunctional analogue H_4neunpa, was synthesized with a general reaction scheme that follows *N*-nosyl protection, bifunctionalization on the middle nitrogen atom via *N*-alkylation, *N*-alkylation with picolinic acid, nosyl deprotection with thiophenol, a second alkyl halide *N*-alkylation, and ester deprotection with LiOH to yield *p*-NO_2−Bn−H_4neunpa **6** (Scheme 1). The isothiocyanate (NCS) analogue for mAb conjugation, *p*-SCN−Bn−H_4neunpa **9**, was synthesized from the intermediate **5** followed by nitro reduction, ester deprotection with LiOH, and isothiocyanate formation with thiophosgene (Scheme 1).

Starting from the diethylenetriamine backbone, the two primary amines were protected with the 2-nitrobenzenesulfonyl groups to yield compound **1**. Compound **1** is highly polar due to the two nosyl groups; thus, a highly polar solvent such as methanol is needed to separate it from the column. The second step is *N*-alkylation with 4-(2-bromoethyl)nitrobenzene. To maintain symmetry of the ligand, the ideal spot for bifunctionalization is the middle nitrogen. After that, *N*-alkylation with methyl-6-bromomethyl picolinate[5] was performed to yield compound **3**. The most challenging step was the nosyl deprotection, constantly resulting in low yields of compound **4**. The deprotected product is unfortunately highly polar and likely adsorbs on the surface of potassium carbonate, as seen by the red color of the salt. It was not possible to

DOI: 10.1021/acs.bioconjchem.7b00311
Bioconjugate Chem. 2017, 28, 2145−2159

Scheme 1. Synthetic Scheme for *p*-SCN−Bn−H_4neunpa and *p*-NO_2−Bn−H_4neunpa

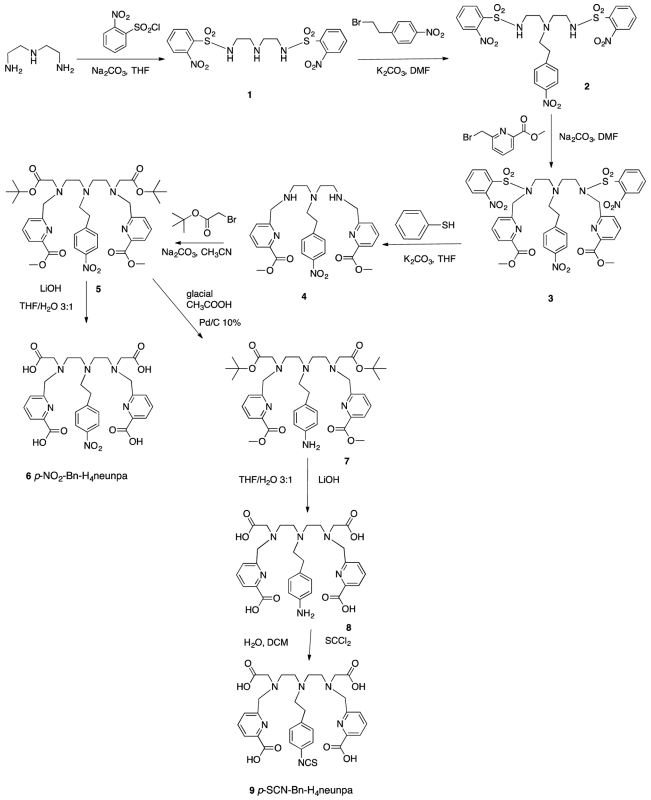

remove the large fractions of the deprotected product completely from the salt, which explains the low yield reported in the Experimental section. Subsequently, alkyl halide *N*-alkylation was performed to yield product **5** with 71% yield. *p*-NO_2−Bn−H_4neunpa **6** was synthesized in a final step of ester deprotection with LiOH. This compound was further used for radiolabeling experiments as well as potentiometric stability titrations. The ^{1}H NMR spectrum of the final product is shown in Figure 2.

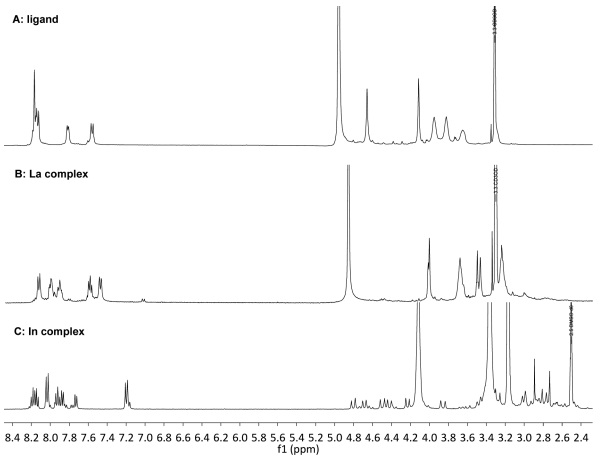

Figure 2. ^{1}H NMR spectra of A: *p*-NO_2−Bn−H_4neunpa-*p*-Bn−NO_2 (400 MHz, $CDCl_3$, 25 °C); B: $[La(p\text{-}NO_2\text{−}Bn\text{−}neunpa)]^-$ (400 MHz, $CDCl_3$, 25 °C); C: $[In(p\text{-}NO_2\text{−}Bn\text{−}neunpa)]^-$ (400 MHz, DMSO-d_6, 25 °C).

p-SCN−Bn−H_4neunpa **9** was synthesized starting from the intermediate **5** of the previous reaction route. Reduction of the nitro group with palladium on carbon yielded the amine-functionalized product **7.** The hydrolysis of the two *tert*-butyl esters and two methyl esters was performed differently from previous reports.[5,12] Instead of acidic hydrolysis at high temperatures, compound **8** was synthesized by adding 10 equiv. of lithium hydroxide to the reaction mixture at room temperature to yield the product with a 50% yield. The final step is the synthesis of the isothiocyanate-functionalized product **9**. This was achieved by the reaction of excess thiophosgene with the aromatic primary amine to yield the final product with a 59% yield. Overall, the synthesis of *p*-SCN−Bn−H_4neunpa from diethylenetriamine has a cumulative yield of 2.3%, comparable to the overall synthesis yield of H_5decapa (2.5%).

Synthesis and Characterization of Nonradioactive Metal Complexes. *NMR.* A total of three complexation experiments were performed with La^{3+}, In^{3+}, and Bi^{3+}. ^{1}H NMR spectra of the *p*-NO_2−Bn−H_4neunpa ligand precursor, and corresponding La and In complexes can be found in Figure 2. The $[La(p\text{-}NO_2\text{−}Bn\text{−}neunpa)]^-$ complex shows ^{1}H NMR upfield shifts of the alkyl region; this effect has been previously observed in our group.[13] The aromatic region is more resolved and shows a splitting of the peaks. Integration of all peaks gives the same number of protons compared to the uncomplexed ligand. Furthermore, the HSQC spectra of this complex (Figure S2) shows the same number of carbons compared to the bare ligand, suggesting that there is only one isomer in solution. In contrast, the ^{1}H NMR spectrum of $[In(p\text{-}NO_2\text{−}Bn\text{−}neunpa)]^-$ shows more splitting in the aromatic and alkyl regions. The aromatic peaks are sharp and well-resolved, and integrating the peaks suggests one major static isomer. In addition, the COSY spectrum of this complex shows clear coupling of several peaks in the complex alkyl region (Figure S12), leading to the assumption that there are fluxional isomers in solution. Comparing these results to those with $[In(decapa)]^{2-}$, which gave a complex ^{1}H NMR spectrum with multiple isomers, presumably due to several unbound carboxylates,[10] we can see an improvement in terms of isomerization by replacing one carboxylate group with the functionalization arm on the middle nitrogen atom of the diethylenetriamine backbone. Due to insolubility of the Bi complex, the ^{1}H NMR spectrum cannot be used for proper assignments (Figure S1).

IR. Due to the insolubility of $[Bi(p\text{-}NO_2\text{−}Bn\text{−}neunpa)]^-$, an infrared (IR) experiment on the solid was performed (Figure 3). Shifts of various peaks of the ligand itself compared to the Bi complex can be observed. The OH stretch at 2500 cm^{-1} disappeared after complexation, suggesting that the carboxylic acids are bound to the metal ion; the carboxyl stretch at 1700 cm^{-1} disappeared as well, supporting this assumption. The two stretches of the nitro functional group (1500 and 1400 cm^{-1}) stayed the same. The stretch at 1200 cm^{-1} in the ligand spectra can be assigned as a C−N stretch that shifts to lower energies (1000 cm^{-1}) when bound to the metal ion.

Thermodynamic Stability. The extended diethylenetriamine backbone, along with the nonadentate N_5O_4 binding motif of H_4neunpa, were specifically designed to accommodate binding of larger metal ions. As such, the protonation constants of H_4neunpa as well as the stability constants of the respective La^{3+}, Bi^{3+}, and In^{3+} complexes were determined at 25 °C in 0.16 M NaCl aqueous solution. The stepwise protonation constants (log *K*) obtained are presented in Table 1, together with

DOI: 10.1021/acs.bioconjchem.7b00311
Bioconjugate Chem. 2017, 28, 2145−2159

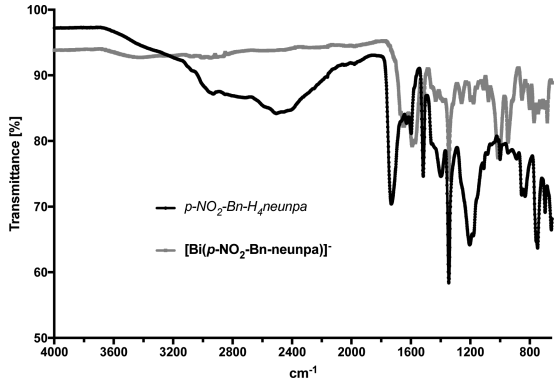

Figure 3. IR spectra of *p*-NO_2−Bn−H_4neunpa and [Bi(*p*-NO_2−Bn−neunpa)]$^-$.

protonation and stability constants reported for the related ligands H_5decapa, H_4octapa, DTPA, and CHX-A″−DTPA. A straightforward comparison of the ability of different ligands to coordinate a specific metal ion (rather than the thermodynamic stability constants alone) is the conditional stability constant or *p*M value. *p*M is defined as (−log $[M^{n+}]_{free}$) and is calculated at specific conditions ($[M^{n+}]$ = 1 μM, $[L^{x-}]$ = 10 μM, pH 7.4 and 25 °C), taking into consideration both metal−ligand association and ligand basicity. The protonation constants of the new synthesized ligand H_4neunpa were determined by potentiometric titrations at pH 1.8−11.5 and by combined potentiometric-spectrophotometric titrations[16,17] over the pH range of 2.5−11.5. In Figure S3 are shown the sets of spectra obtained as a function of pH at 7.18 × 10^{-4} M ligand concentration. The first and second protonation processes occur at the two terminal amines of the diethylenetriamine backbone (log K_1 = 10.92(2) and log K_2 = 9.29(2)), as suggested by the appearance of a single isosbestic point at 284 nm between pH 8.33 and 11.32 in the UV-potentiometric titration (Figure S3c). The third protonation process (log K_3 = 6.79(2)) is assigned to the central nitrogen atom in the backbone and is supported by the appearance of an isosbestic point at 293 nm in the pH region between 5.39 and 8.33 (Figure S3b). The fourth and fifth protonation processes are attributed to the picolinate moieties[13,18] (log K_4 = 4.02(3) and log K_5 = 2.97(2)). The UV-potentiometric titration showed also in this case a single isosbestic point at 296 nm for these protonation processes (Figure S3a). The sixth protonation step is attributable to the carboxylic acid substituent (log K_6 = 2.39(5)) and was calculated from potentiometric titrations. The value of log K_7 could not be determined, as the value was below the threshold of the electrode (pH < 2). H_4neunpa, the bifunctional analogue of the previously reported H_5decapa (for which we correct here the protonation constants, Table 1) presents overall fairly similar protonation constants, although the fourth and fifth protonation processes attributed to the picolinate moieties differ by 0.41 and 0.49 units, respectively. The higher protonation constants in the case of H_5decapa could be attributed to the higher negative charge of the ligand. The speciation plots for H_4neunpa and H_5decapa are shown in Figure S4.

Potentiometric titrations of H_4neunpa were carried out in the presence of La^{3+}, Bi^{3+}, and In^{3+} to determine the stability constants of the corresponding metal complexes. For lanthanum, combined potentiometric−spectrophotometric titrations demonstrated that the complexation started from pH 2, determined based on the distinctive features of the spectra compared to the electronic spectra of H_4neunpa (Figures S3 and S5). The thermodynamic stability of [La(neunpa)]$^-$ was determined to be log K_{ML} = 19.81(4) and pM = 16. This value is close to the values obtained for [La(octapa)]$^-$ log K_{ML} = 19.92(6)[19] and [La(DTPA)]$^{2-}$ log K_{ML} = 19.48.[20] Similar to the free ligand, the deprotonation of the [La(H_2neunpa)]$^+$ and La(Hneunpa) species is marked by the appearance of a single isosbestic point at 291 nm between the pH range of 2.42−8.23 and suggests that the deprotonations occur at the two terminal amines of the diethylenetriamine backbone (Figure S5a). The [La(neunpa)]$^-$ species further deprotonates presumably due to the deprotonation of a coordinated water molecule with p*K* 9.78 to form the monohydroxo complexes (Figure S5b). Species-distribution diagrams for the lanthanum(III) complexes of H_4neunpa are plotted in Figure S6. The thermodynamic stability constant of the bismuth(III) complexes of H_4neunpa could not be determined by direct potentiometric titrations because this requires the knowledge of the concentration of the free and bound metal ion at equilibrium, and even at pH 2, the Bi(III) complex was already significantly formed. The ligand−ligand competition method using Na_2H_2EDTA as a known competitor was used to yield the stability constants presented in Table 2 and the speciation plots in Figure S7. The particularly high thermodynamic stability of [Bi(neunpa)]$^-$ was found: log K_{ML} = 28.76(9) and pBi = 27. The thermodynamic stability constant of the [Bi(neunpa)]$^-$ complex is lower than those of [Bi(DTPA)]$^{2-}$ and [Bi(CHX-A−DTPA)]$^{2-}$ complexes[14] and lower than that for [Bi(DOTA)]$^-$; however, it is interesting to note that H_4neunpa and DOTA have the same pBi^{3+} value of 27 (Table 2). Despite the high formation constant of [In(H_2neunpa)]$^{2+}$ log K_{MLH2} = 36.64(3), the system is well-determined by direct potentiometric titration taking advantage of the indium−chloride competing species.

Table 1. Stepwise Protonation Constants (log K_{HhL}) of H_4neunpa (25 °C, *I* = 0.16 M NaCl)[a]

equilibrium reaction	neunpa^{4-} (this work)	decapa^{5-} (this work)	octapa^{4-}[10]	DTPA[14]	CHX-A″−DTPA[14]	DOTA[15]
L + H^+ ⇆ HL	10.92(2)	11.03(3)	8.59(4)	11.84	12.30	12.60(1)
HL + H^+ ⇆ H_2L	9.29(2)	9.20(3)	5.59(6)	9.40	9.24	9.70(1)
H_2L + H^+ ⇆ H_3L	6.79(2)	6.86(4)	3.77(2)	4.85	5.23	4.50(1)
H_3L + H^+ ⇆ H_4L	4.02(3)	4.43(4)	2.77(4)	3.10	3.32	4.14(1)
H_4L + H^+ ⇆ H_5L	2.97(2)	3.46(5)	2.79(4)	2.20	2.18	2.32(1)
H_5L + H^+ ⇆ H_6L	2.39(5)	2.84(6)	ND			
H_6L + H^+ ⇆ H_7L	ND	2.52(4)				
H_7L + H^+ ⇆ H_8L		ND				

[a]Literature data of related systems are presented for comparison. L indicates ligand; charges of ligand species and metal complexes were omitted for simplicity.

DOI: 10.1021/acs.bioconjchem.7b00311
Bioconjugate Chem. 2017, 28, 2145−2159

Table 2. Stepwise Stability Constants (log K) of H_4neunpa Complexes with La^{3+}, Bi^{3+}, and In^{3+}[a]

equilibrium reaction	neunpa^{4-}	decapa^{5-}[10]	octapa^{4-}	DTPA	CHX-A″−DTPA	DOTA
$La^{3+} + L \leftrightarrows LaL$	19.81(4)		19.92(6)[19]	19.48[20]		22.0[21]
$LaL + H^+ \leftrightarrows LaHL$	8.05(5)					
$LaHL + H^+ \leftrightarrows LaH_2L$	3.28(6)					
$LaLOH + H^+ \leftrightarrows LaL$	9.78(4)					
$Bi^{3+} + L \leftrightarrows BiL$	28.76(9)			35.2(4)[14]	34.9(4)[14]	30.3[22]
$BiL + H^+ \leftrightarrows BiHL$	10.26(5)					
$BiHL + H^+ \leftrightarrows BiH_2L$	3.8(1)					
$BiLOH + H^+ \leftrightarrows BiL$	10.57(7)					
$In^{3+} + L \leftrightarrows InL$	28.17(2)	27.56(5)	26.8(1)[10]	29.0[23,24]		23.9(1)[24]
$InL + H^+ \leftrightarrows InHL$	5.07(2)	5.47(3)	2.9(2)[10]			
$InHL + H^+ \leftrightarrows InH_2L$	3.40(3)	2.73(6)				
$InLOH + H^+ \leftrightarrows InL$	9.41(3)	9.83(7)				
pLa^{3+}	16		19.7			
pBi^{3+}	27					27[25]
pIn^{3+}	23.6	23.1	26.5[10]	25.7[10]		18.8[10]

[a]Literature data for related systems are presented for comparison. L indicates ligand; charges of ligand species and metal complexes were omitted for simplicity.

The system as in the case of lanthanum(III) and bismuth(III) complexes containing MLH_2, MLH, ML, and ML(OH) complex species (Figure S8) presented a high log K_{ML} = 28.17(2) and pM = 23.6, which is significantly higher than for DOTA (Table 2), slightly higher than for the previously reported H_5decapa, 2.1 pM units lower than for DTPA and 2.9 pM units lower than for $[In(octapa)]^-$. To our knowledge, thermodynamic formation constants of the $[In(CHX\text{-}A''\text{−}DTPA)]^{2-}$ have not been yet reported. It is noteworthy that, as with other previously reported ligands,[10] the trend of the stability constants and pM values and the human serum stability data do not correlate well, and despite the higher pM values for $[In(octapa)]^-$ species or $[In(DTPA)]^{2-}$ versus $[In(neunpa)]^-$, $[In(neunpa]^-$ showed an exceptional serum stability 97.8(1) % after 1 day, 5.5 units higher than the $[In(octapa)]^-$ complex, 7.9 units higher than the $[In(CHX\text{-}A''\text{−}DTPA)]^{2-}$ complex and 9.5 units higher than the $[In(DTPA)]^{2-}$ complex.

Radiolabeling Experiments with Unmodified Chelators. The radiolabeling properties of ^{177}Lu and ^{111}In with H_4neunpa were investigated, and compared directly to results obtained for the gold standards DOTA and CHX-A″−DTPA. Initial radiolabeling experiments revealed that p-NO_2−Bn−H_4neunpa could quantitatively complex $^{111}In^{3+}$ (radiochemical yield, RCY > 99%) in 10 min at room temperature (rt), pH 4, at ligand concentrations of 10^{-4} M. Subsequently, concentration-dependent labeling was performed by decreasing the ligand concentration 10-fold while keeping the ^{111}In activity constant. Quantitative radiolabeling was achieved at ligand concentrations as low as 10^{-7} M (Figure 4) at 10 min and ambient temperature. At decreasing ligand concentrations of 10^{-8}, 10^{-9}, and 10^{-10} M, radiochemical yields gradually decreased to 71.1, 10.5, and 1.5%, respectively. These results demonstrate the ability of p-NO_2−Bn−H_4neunpa to rapidly and efficiently complex ^{111}In in highly specific activities at ambient temperatures. H_4octapa showed similar radiolabeling efficiencies at 10^{-7} M, and results at lower ligand concentrations are not reported.[10] In sharp contrast to the two "pa" ligands is the macrocyclic gold standard DOTA, which is reported to require heating samples at 100 °C for 30 min to achieve high radiochemical yields.[10] The acyclic chelator CHX-A″−DTPA is a relatively recent addition to the list of potential ^{111}In chelators; in contrast to DOTA, it can efficiently complex In^{3+} isotopes at ambient temperatures yet exhibits comparable in vivo stability to DOTA conjugates,[2,26] making it a more-appealing chelator for radiolabeling of heat-sensitive biomolecules such as affibodies or antibodies.[27−31] Our initial ^{111}In radiolabeling studies with p-NH_2−Bn−CHX-A″−DTPA at ligand concentrations of 10^{-4} M corroborate the efficient and mild labeling of this ligand, which yielded RCYs > 99%; however, two evident peaks in the HPLC radio-chromatogram are observed, one major product at 8.6 min and a minor product at 8.0 min (Figure S10), with the ratio between the major and minor product being 7.7. The appearance of two distinct peaks in the radio-chromatogram may indicate the formation of distinct ^{111}In−chelate isomers. Contrary to H_4neunpa, at p-NH_2−Bn−CHX-A″−DTPA concentrations of 10^{-7} and 10^{-8} M, ^{111}In labeling yield decreased to 75.0 and 3.4%, respectively. The ratio of major to minor product in the HPLC radio-chromatogram also changed drastically at lower ligand concentrations, with the ratio being close to unity (0.95) for 10^{-7} M labeling.

Unlike the facile labeling kinetics of $[^{111}In(p\text{-}NO_2\text{−}Bn\text{-}neunpa)]^-$, initial radiolabeling studies with ^{177}Lu were unsuccessful. Attempted ^{177}Lu labeling at ligand concentrations of 10^{-4} M in 10 min at room temperature, pH 4 or 5.5, displayed a radiochemical yield of 12.4%; heating the sample to 40 °C for 1 h did not improve RCY. Conversely, gold-standard DOTA was quantitatively radiolabeled (RCY > 99%) with ^{177}Lu when heated to 40 °C for 1 h at the same ligand concentration (10^{-4} M). The inability of p-NO_2−Bn−H_4neunpa to complex ^{177}Lu isotopes at mild temperatures

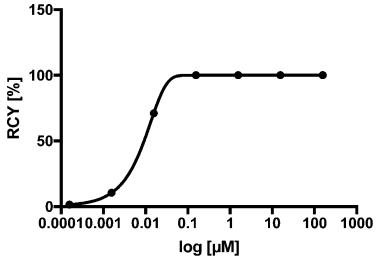

Figure 4. Radiolabeling results of ^{111}In−p-NO_2−Bn−neunpa (10 min, RT, pH 4).

DOI: 10.1021/acs.bioconjchem.7b00311
Bioconjugate Chem. 2017, 28, 2145−2159

(<40 °C) precluded further study with this isotope because it was immediately obvious from the initial results that H_4neunpa was a poor match for ^{177}Lu and presented no potential advantage compared to the gold-standard DOTA.

Stability Studies with the Unmodified Chelators. To probe the kinetic inertness of the [^{111}In(*p*-NO_2−Bn−neunpa)]$^-$ complex, a 5 day in vitro competition experiment was performed in the presence of human blood serum. Serum contains many endogenous ligands that can compete for In(III) binding in vivo, such as *apo*-transferrin and albumin, and any chelate-bound ^{111}In must therefore be sufficiently stable to withstand transchelation to such proteins. The in vitro stability of [^{111}In(*p*-NO_2−Bn−neunpa)]$^-$ at the 1 h and 1 and 5 day time points was tested alongside gold-standard [^{111}In(*p*-NH_2−Bn−CHX-A″−DTPA)]$^{2-}$ for comparison (Table 3). The

Table 3. Human Serum Stability Challenge Data Performed at 37 °C (n = 3), with Stability Shown as Percentage of Intact ^{111}In Complex

complex	1 h (%)	1 day (%)	5 day (%)
[^{111}In(*p*-NO_2−Bn−neunpa)]$^-$	97.9 ± 0.3	97.8 ± 0.1	97.8 ± 0.7
[^{111}In(*p*-NH_2−Bn−CHX-A″−DTPA)]$^{2-}$	91.8 ± 1.8	89.9 ± 0.6	90.1 ± 0.9
[^{111}In(octapa)]$^-$[a]	93.8 ± 3.6	92.3 ± 0.04	ND[b]
[^{111}In(DOTA)]$^-$[a]	89.6 ± 2.1	88.3 ± 2.2	ND[b]
$^{111}InCl_3$ (control)[c]	4.0	7.2	3.4

[a]Mouse serum stability data performed at ambient temperature; data included from ref 10 for comparison. [b]ND: not determined. [c]n = 1 only.

[^{111}In(*p*-NO_2−Bn−neunpa)]$^-$ complex exhibited exceptional stability, remaining 97.8% intact over 5 days, while the [^{111}In(*p*-NH_2−Bn−CHX-A″−DTPA)]$^{2-}$ complex showed an initial ∼8% drop in stability after 1 h and subsequently stabilized for 5 days to remain 90.1% intact. The initial drop in stability after 1 h may be due to the presence of two isomers in the labeling reaction of *p*-NH_2−Bn−CHX-A″−DTPA (vide supra, major isomer 88.5% and minor isomer 11.5%). Studies with ^{88}Y−CHX−DTPA have demonstrated that thermodynamic stability of the resultant metal complex can be significantly affected by the absolute configuration, possibly due to unfavorable steric hindrance of certain stereoisomers;[32] therefore, it is feasible that the minor isomer is kinetically labile with respect to transchelation to serum proteins. Indeed, [^{111}In(*p*-NO_2−Bn−neunpa)]$^-$ displayed marginally higher stability than [^{111}In(*p*-NH_2−Bn−CHX-A″−DTPA)]$^{2-}$, [^{111}In(DOTA)]$^-$, and [^{111}In(octapa)]$^-$ after 1 day (97.8 ± 0.1%, 89.9 ± 0.6, 88.3 ± 2.2%, and 92.3 ± 0.04%, respectively).

Initial Biodistribution Studies. Mouse biodistribution studies over the course of 24 h (n = 4 each time point) were performed with [^{111}In(*p*-NO_2−Bn−neunpa)]$^-$ and [^{111}In(*p*-NH_2−Bn−CHX-A″−DTPA)]$^{2-}$, and the data are summarized in Table 4. Both In complexes were rapidly excreted through the kidneys and activity cleared quickly from all other organs. Notably, uptake of [^{111}In(*p*-NO_2−Bn−-neunpa)]$^-$ in the intestines was significantly higher than for [^{111}In(*p*-NH_2−Bn−CHX-A″−DTPA)]$^{2-}$ after 15 min (17.9 ± 5.5 versus 3.6 ± 1.6 percent of the injected dose per gram of tissue [% ID/g]) and 1 h (39.8 ± 2.9 versus 10.7 ± 1.4% ID/g). One explanation for the difference in intestine uptake is that the monoanionic ^{111}In-neunpa complex is more lipophilic than the dianionic ^{111}In−*p*-NH_2−Bn−CHX-A″−DTPA complex, as evidenced by shifts in the radio-high-performance liquid chromatography (HPLC) retention times (t_R = 12.9 and 8.6 min, respectively) and the absolute log *p* values of each complex (−1.65 ± 0.04 and −3.85 ± 0.17, respectively), thus shifting the excretion of the radiotracer from renal to intestinal elimination because highly charged polar substances are generally eliminated via the kidneys, while less-hydrophilic compounds tend to be eliminated via the intestinal tract. Nonetheless, the remaining ^{111}In complex in the intestines at 1 h was rapidly excreted by 4 h for both complexes, and the uptake in intestines of [^{111}In(*p*-NO_2−Bn−neunpa)]$^-$ and [^{111}In(*p*-NH_2−Bn−CHX-A″−DTPA)]$^{2-}$ were no longer statistically different (p > 0.05) at later time points (0.265 ± 0.206 versus 0.160 ± 0.047% ID/g for 4 h and 0.216 ± 0.114 versus 0.129 ± 0.06% ID/g for 24 h, respectively). It has been suggested that administration of an unstable ^{111}In complex would result in demetalation of the complex in vivo and subsequent accumulation of transchelated or "free" $^{111}In^{3+}$ activity in the liver, spleen, and bone over time;[33] therefore, the rapid excretion of [^{111}In(*p*-NO_2−Bn−neunpa)]$^-$ and [^{111}In(*p*-NH_2−Bn−CHX-A″−DTPA)]^2 from these organs suggests that both ^{111}In complexes are exceptionally robust and stable in vivo (0.035 ± 0.008 versus 0.023 ± 0.006% ID/g for liver; 0.029 ± 0.01 versus 0.032 ± 0.008% ID/g for spleen; and 0.010 ± 0.006 versus 0.007 ± 0.002% ID/g for bone, at 24 h, respectively). Furthermore, [^{111}In(*p*-NO_2−Bn−neunpa)]$^-$ had improved kidney clearance compared to [^{111}In(*p*-NH_2−Bn−CHX-A″−DTPA)]$^{2-}$ at 24 h (0.077 ± 0.058 versus 0.301 ± 0.043% ID/g, respectively; p < 0.05). Although these initial biodistribution data appear promising it may be that the predicted −1 and −2 charge of the In-neunpa and −CHX-A″−DTPA complexes, respectively, at physiological pH, could be mediating the rapid elimination of the metal complexes from the body; therefore, the In complexes may not have ample opportunity to dissociate in vivo, giving the appearance of a stable complex. To further scrutinize the in vivo stability of ^{111}In-neunpa and ^{111}In−CHX-A″−DTPA, an immunoconjugate should be prepared (vide infra) and, accordingly, biodistribution of each complex can be monitored over the course of several days instead of hours.

Preparation of Bioconjugates and in Vitro Characterization. The promising radiolabeling efficiencies and in vitro kinetic inertness of [^{111}In(*p*-NO_2−Bn−neunpa)]$^-$ provided motivation to prepare and test the radiolabeling properties and the in vivo behavior of a H_4neunpa bioconjugate. The HER2/*neu*-targeting antibody trastuzumab was chosen as the biovector because it is well-established to target HER2-expressing tumors such as the SKOV-3 ovarian cancer cell line. To provide a basis for comparison, the gold standard CHX-A″−DTPA was also conjugated to trastuzumab and tested in parallel in the radiolabeling and in vivo experiments.

The novel bifunctional chelator *p*-SCN−Bn−H_4neunpa **9** and gold standard *p*-SCN−Bn−CHX-A″−DTPA were conjugated to trastuzumab by incubation at room temperature at a 5:1 molar ratio of ligand to antibody under slightly basic conditions (pH 9.0).[34] Final immunoconjugates were purified by spin-filtration and stored at −20 °C until use. A radiometric isotopic dilution assay was employed to determine the number of accessible chelates per antibody; an average of 5.5 ± 1.1 H_4neunpa chelates per antibody and 4.6 ± 0.7 CHX-A″−DTPA chelates per antibody were conjugated to trastuzumab.

Preliminary ^{111}In radiolabeling efficiency of H_4neunpa−trastuzumab was tested at pH 5.0, 5.5, and 6.0 in NH_4OAc buffer (0.15 M) at rt, and the radiochemical yield was assessed

DOI: 10.1021/acs.bioconjchem.7b00311
Bioconjugate Chem. 2017, 28, 2145−2159

Table 4. Decay-Corrected Percent ID/g Values from Biodistribution of ^{111}In Complexes in Healthy NOD.Cg-Prkdc^{scid} Il2rg^{tm1Wjl}/SzJ Female NOD.Cg-Prkdc^{scid} Il2rg^{tm1Wjl}/SzJ Mice (4 Months Old)[a]

organ	15 min	1 h	4 h	24 h
		[^{111}In][In(*p*-NO_2−Bn−neunpa)]$^-$		
blood	1.979 (0.425)	0.077 (0.007)	0.022 (0.004)	**0.0064 (0.0011)**
fat	0.174 (0.113)	0.009 (0.001)	0.0020 (0.0009)	0.0009 (0.0007)
uterus	1.644 (0.321)	0.101 (0.011)	0.059 (0.072)	**0.014 (0.005)**
ovaries	0.983 (0.362)	0.056 (0.034)	0.012 (0.011)	**0.0080 (0.0067)**
intestine	**17.941 (5.475)**	**39.760 (2.865)**	0.265 (0.206)	0.216 (0.114)
spleen	0.792 (0.379)	0.073 (0.024)	0.032 (0.027)	0.029 (0.010)
liver	**2.684 (0.190)**	0.312 (0.090)	0.071 (0.016)	0.035 (0.008)
pancreas	0.287 (0.196)	0.026 (0.006)	0.010 (0.006)	0.0047 (0.0023)
stomach	1.251 (0.364)	0.054 (0.019)	**0.012 (0.002)**	0.062 (0.019)
adrenal glands	0.585 (0.089)	0.037 (0.029)	0.012 (0.010)	**0.0009 (0.0018)**
kidney	5.681 (1.343)	**0.484 (0.322)**	**0.158 (0.105)**	**0.077 (0.058)**
lungs	**2.695 (0.392)**	0.388 (0.526)	0.072 (0.101)	0.056 (0.096)
heart	**0.419 (0.032)**	0.075 (0.089)	0.011 (0.007)	0.0061 (0.0103)
muscle	0.394 (0.101)	0.016 (0.004)	0.0030 (0.0018)	0.0020 (0.0016)
bone	0.743 (0.351)	0.072 (0.029)	0.0099 (0.0069)	0.0102 (0.0060)
brain	0.059 (0.033)	0.012 (0.002)	**0.0013 (0.0006)**	0.0009 (0.0016)
tail	4.129 (2.183)	**0.143 (0.095)**	0.029 (0.023)	**0.0078 (0.0060)**
		[^{111}In][In(*p*-NH_2−Bn−CHX-A″−DTPA)]$^{2-}$		
blood	2.370 (0.221)	0.091 (0.035)	0.013 (0.014)	**0.0011 (0.0003)**
fat	0.323 (0.070)	0.016 (0.007)	0.0037 (0.0014)	0.0024 (0.0017)
uterus	1.643 (0.121)	0.116 (0.045)	0.082 (0.092)	**0.035 (0.007)**
ovaries	1.279 (0.177)	0.077 (0.033)	0.024 (0.016)	**0.0188 (0.0047)**
intestine	**3.644 (1.632)**	**10.713 (1.428)**	0.160 (0.047)	0.129 (0.060)
spleen	0.627 (0.069)	0.074 (0.031)	0.036 (0.008)	0.032 (0.008)
liver	**3.388 (0.293)**	0.271 (0.093)	0.053 (0.005)	0.023 (0.006)
pancreas	0.539 (0.148)	0.036 (0.017)	0.014 (0.009)	0.0053 (0.0020)
stomach	1.037 (0.115)	0.058 (0.025)	**0.018 (0.003)**	0.042 (0.030)
adrenal glands	0.592 (0.174)	0.064 (0.048)	0.022 (0.003)	**0.0156 (0.0043)**
kidney	7.643 (1.741)	**1.152 (0.276)**	**0.632 (0.076)**	**0.301 (0.043)**
lungs	**1.677 (0.227)**	0.120 (0.045)	0.023 (0.003)	0.012 (0.002)
heart	**0.697 (0.089)**	0.041 (0.013)	0.011 (0.001)	0.0069 (0.0011)
muscle	0.500 (0.122)	0.022 (0.008)	0.0038 (0.0003)	0.0016 (0.0007)
bone	0.717 (0.187)	0.057 (0.011)	0.0112 (0.0014)	0.0066 (0.0015)
brain	0.063 (0.018)	0.017 (0.004)	**0.0068 (0.0008)**	0.0018 (0.0006)
tail	3.562 (1.334)	**0.349 (0.063)**	0.410 (0.498)	**0.0505 (0.0324)**

[a] $n = 4$; statistical analysis,Student's T-test; bold indicates $p < 0.05$.

Table 5. Chemical and in Vitro Characterization Data of ^{111}In-neunpa−/−CHX-A″−DTPA−Trastuzumab Radioimmunoconjugates

immunoconjugate	radiolabeling conditions and yield	chelate/mAb	specific activity (mCi/mg)	immunoreactive fraction (%)	serum stability over 5 days (%)
^{111}In-neunpa−trastuzumab	pH 6, rt, 15 or 30 min, 92.6%	5.5 ± 1.1	28.0	>99	94.7%
^{111}In−CHX-A″-DTPA−trastuzumab	pH 6, rt, 30 min, 91.6%	4.6 ± 0.7	20.8	>99	ND

at 15 min. Calculated RCYs after 15 min were 15.0, 84.4, or 92.6% at pH 5.0, 5.5, or 6.0, respectively (Figure S11). RCY was also assessed after 90 min for pH 5.0 and 6.0 reactions; yields increased to 38% and remained constant at 92% for pH 5.0 and 6.0, respectively. These initial radiolabeling tests suggest an optimal radiolabeling pH of 6.0 for H_4neunpa−trastuzumab to generate ^{111}In conjugates of high radiochemical yield (>90%) and purity in only 15 min at rt. This is in agreement with a solution equilibrium study, which reflects the maximum of the [In(neunpa)]$^-$ species formed at pH 6 (see the distribution diagram in Figure S7). The kinetic inertness of ^{111}In-neunpa−trastuzumab was assessed in an in vitro human serum challenge assay at 37 °C. Much like the unconjugated precursor, ^{111}In-neunpa−trastuzumab was exceptionally inert to transchelation when incubated with human serum, with 95.0 ± 1.1, 96.0 ± 2.5, 94.7 ± 0.6, and 94.8 ± 1.6% of the ^{111}In bioconjugate remaining intact after 1, 2, 5, and 7 days, respectively.

^{111}In-labeled trastuzumab conjugates were then prepared for in vivo studies. Both immunoconjugates were radiolabeled with ^{111}In in NH_4OAc buffer (0.15 M, pH 6) for 30 min at rt (Table 5), resulting in exceptionally high radiochemical yields (>90%) and radiochemically pure products (>99% after spin purification) for both ^{111}In-neunpa−trastuzumab and ^{111}In−CHX-A″−DTPA−trastuzumab. Final specific activities were determined to be 28.0 and 20.8 mCi/mg (1036 and 770 MBq/

DOI: 10.1021/acs.bioconjchem.7b00311
Bioconjugate Chem. 2017, 28, 2145−2159

mg) for ^{111}In-neunpa−trastuzumab and ^{111}In−CHX-A″−DTPA−trastuzumab, respectively. In vitro cellular binding assays with SKOV-3 cancer cells showed both ^{111}In immunoconjugates absolutely reactive toward the tested cell line (>99% immunoreactivity). Both ^{111}In immunoconjugates have thus the ability to still bind to HER2.

Biodistribution and SPECT−CT Imaging Studies. To compare directly the pharmacokinetics of ^{111}In-neunpa−trastuzumab to ^{111}In−CHX-A″−DTPA−trastuzumab in vivo, biodistribution and single photon emission computed tomography in conjunction with helical X-ray CT imaging experiments were performed on female mice bearing subcutaneous SKOV-3 ovarian cancer xenografts on the left shoulder. Either tracer was injected via the tail vein (~37 MBq, ~35−50 μg, in 200 μL of saline), and after 1, 3, and 5 days (n = 4 per time point), the mice were imaged (n = 2, Figure 4) and sacrificed to collect organs and tumors to be counted on a calibrated γ-counter.

SPECT−CT overlays of ^{111}In−CHX-A″−DTPA−trastuzumab and ^{111}In-neunpa−trastuzumab immunoconjugates are shown in Figure 5 at 1, 3, and 5 days post-injection. These

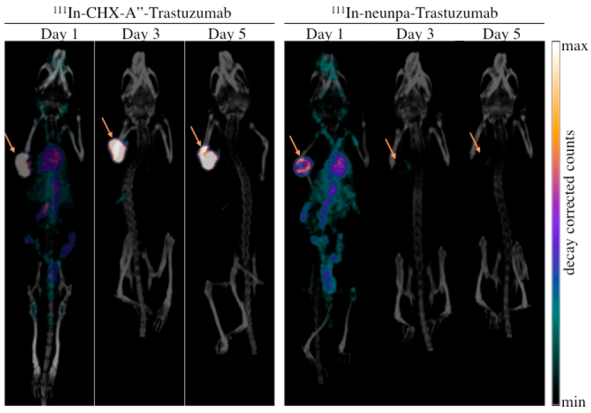

Figure 5. SPECT−CT overlays of ^{111}In−CHX-A″−DTPA−trastuzumab (left) and ^{111}In-neunpa−trastuzumab immunoconjugates. Fused μSPECT−CT images in female mice with subcutaneous SKOV-3 xenografts on left shoulder, imaged at 1, 3, and 5 days post-injection. Tumors are highlighted with arrows.

images were corrected for decay to allow qualitative comparison for the two radiolabeled immunoconjugates. For ^{111}In−CHX-A″−DTPA−trastuzumab and ^{111}In-neunpa−trastuzumab, day 1 images show significant activity in the blood, the heart, the spleen, and the tumor. The activity in the blood, the heart, and the spleen decreases over time. The ^{111}In−CHX-A″−DTPA−trastuzumab shows a higher activity in the tumor at all three time points, giving highly localized activity to the tumor site. However, ^{111}In-neunpa−trastuzumab shows a lower uptake of activity into the tumor at day one post-injection. Over time, the activity in the tumor decreased to being barely visible after 5 days post-injection. Activity in the tumors for the ^{111}In-neunpa−trastuzumab (Figure 5) is still present at day 3 and 5 post-injection, but to be able to compare the two tracers, an appropriate scale bar was required to prevent oversaturation of the high uptake of the ^{111}In−CHX-A″−DTPA−trastuzumab within tumors. Reducing the max value of the scale bar by a factor of 2.8 shows the remaining activity within the tumors for the ^{111}In-neunpa−trastuzumab (data not shown).

Comparing the biodistribution pattern of ^{111}In-neunpa−trastuzumab with ^{111}In−CHX-A″−DTPA−trastuzumab, it is clear that both tracer bioconjugates show the same general uptake profile, i.e. significant uptake in blood, spleen, liver, kidney, bone, and tumor at day 1 (Figure 6 and Table S1). A

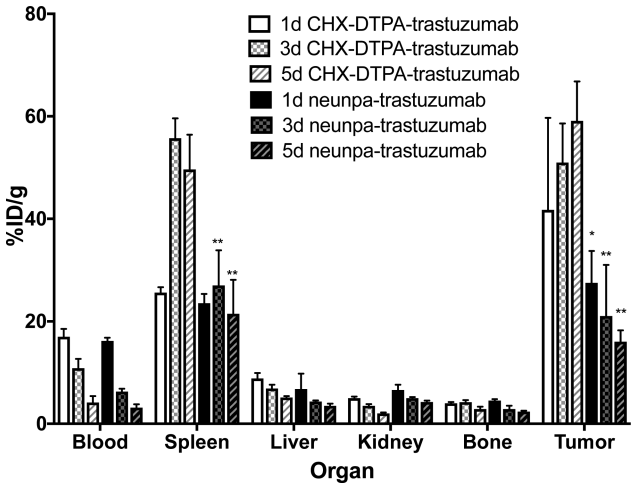

Figure 6. Biodistribution of ^{111}In−CHX-A″−DTPA−trastuzumab compared to ^{111}In-neunpa−trastuzumab in specific organs. Data are expressed as mean ± SD (n = 4). Statistical analysis: a single asterisk indicates $p \leq 0.05$, and two asterisks indicate $p \leq 0.01$; two-way ANOVA.

total of 3 and 5 days after immunoconjugate injection, the spleen and tumor still have the highest uptake of radiotracer compared to all other organs but with significant difference ($p < 0.01$) between ^{111}In−CHX-A″−DTPA−trastuzumab and ^{111}In-neunpa−trastuzumab (49.65 ± 6.79% ID/g for ^{111}In−CHX-A″−DTPA−trastuzumab and 21.47 ± 6.61 %ID/g for ^{111}In-neunpa−trastuzumab after 5 days in the spleen and 59.14 ± 7.70% ID/g for ^{111}In−CHX-A″−DTPA−trastuzumab and 16.01 ± 2.24 %ID/g for ^{111}In-neunpa−trastuzumab after 5 days in the tumor). This distribution of antibody-linked tracer is well-known and is due to the metabolism and circulation of antibodies (or antibody−chelate conjugates).[35]

The blood, liver, kidney, and bone show the lowest percent ID/g regarding all the different organs. The blood from ^{111}In-neunpa−trastuzumab-treated mice is cleared faster than the gold-standard ^{111}In−CHX-A″−DTPA−trastuzumab between 1 and 3 days. Additionally, ^{111}In−CHX-A″−DTPA−trastuzumab shows an increase in accumulation in the tumor over time, whereas ^{111}In-neunpa−trastuzumab shows a decrease of uptake into the tumor over time, which is consistent with the SPECT−CT overlay observations. Regarding the tumor-to-organ ratios (Figure 7), ^{111}In-neunpa−trastuzumab and ^{111}In−CHX-A″−DTPA−trastuzumab interestingly show only significant different values 5 days after injection for each ratio: tumor-to-blood, tumor-to-heart, and tumor-to-muscle. Furthermore, the addition of the several chelating ligands onto trastuzumab (5.5 ± 1.1 H_4neunpa chelates per antibody and 4.6 ± 0.7 CHX-A″−-DTPA chelates per antibody) can modify the overall charge of the antibody. Specifically, one negative charge per $[In(neunpa)]^-$ complex and two negative charges per $[In(CHX-A''-DTPA)]^{2-}$ complex labeled with trastuzumab is generated; this induces a 2-fold increase of negative charge on the CHX-A″−DTPA−trastuzumab conjugates compared to neunpa−trastuzumab conjugates, assuming that an equal number of

DOI: 10.1021/acs.bioconjchem.7b00311
Bioconjugate Chem. 2017, 28, 2145−2159

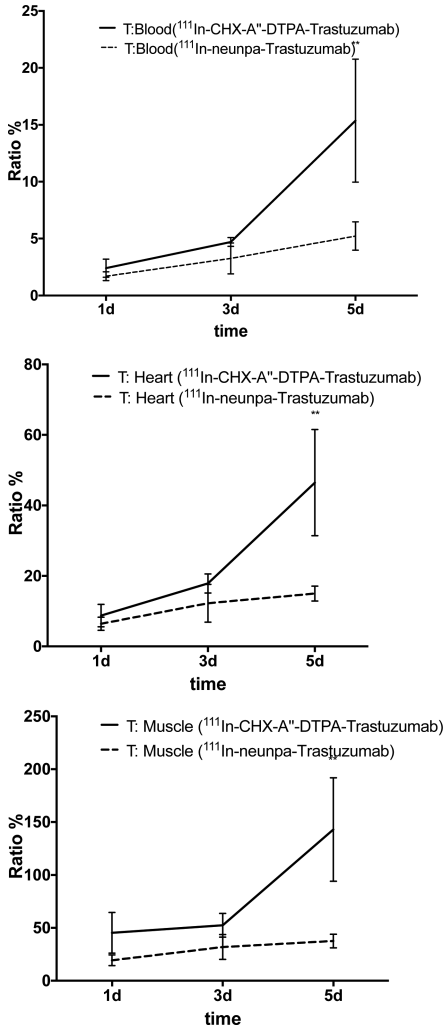

Figure 7. Tumor-to-organ ratios of CHX-A″−DTPA and neunpa. Data are expressed as mean ± SD (n = 4). Statistical analysis: two asterisks indicate $p \leq 0.01$; two-way ANOVA.

accessible chelates are occupied by In^{3+} in each immunoconjugate. Consequently, this variance in overall charge of the trastuzumab conjugate might affect the biodistribution of the resultant ^{111}In tracer. The immunoreactivity results are comparable for H_4neunpa− and CHX-A″−DTPA−trastuzumab conjugates, showing that the reactivity between trastuzumab and its receptor is not altered due to the structural modification after chelate conjugation. We wonder if the stability of the trastuzumab-receptor complex might not be as stable because of the charge difference discussed before. This could lead to a decreased uptake into the cancer cells. In conclusion, from these observations, it was determined that different pharmacokinetic mechanisms for ^{111}In-neunpa−trastuzumab and ^{111}In−CHX-A″−DTPA−trastuzumab might take place after 5 days. These differences will be investigated further to fully understand the mechanism of tumor uptake.

The slightly inferior uptake for this radiometal−neunpa antibody conjugate is disappointing, but the complete chemistry and biology results suggest strongly that H_4neunpa is an attractive chelating ligand with a built-in conjugatable moiety and should be investigated further with Bi^{3+} and in other In^{3+} biovector conjugates.

CONCLUSIONS

The acyclic chelator p-NO_2−Bn−H_4neunpa and the bioconjugated analogue H_4neunpa−trastuzumab (5.5 ± 1.1 chelates per antibody) have been synthesized, characterized (high-resolution electrospray ionization mass spectrometry [HR-ESI-MS], ^{1}H nuclear magnetic resonance [NMR], ^{13}C NMR, 2D-heteronuclear single quantum coherence [HSQC] and cold metal complexation studies) and evaluated via radiolabeling with ^{111}In and ^{177}Lu. Unfortunately, low radiochemical yields of p-NO_2−Bn-H_4neunpa with ^{177}Lu were obtained (pH 4−5.5, ambient −40 °C, max. RCY 12.4%). The radiolabeling yields of p-NO_2−Bn−H_4neunpa and H_4neunpa−trastuzumab with ^{111}In were a great success, >99% and 92.6%, respectively. Human serum stability experiments revealed that the [^{111}In(p-NO_2−Bn−neunpa)]$^-$ complex and ^{111}In-neunpa−trastuzumab immunoconjugate were 97.8 and 94.7% intact after 5 days, respectively. H_4neunpa−trastuzumab was highly immunoreactive (>99%), as indicated by a cellular binding assay. Biodistribution study of [^{111}In(p-NO_2−Bn−neunpa)]$^-$ in mice showed higher uptake into the intestine within the first hours compared to [^{111}In(CHX-A″−DTPA)]$^{2-}$ due to its higher lipophilicity. Small-animal SPECT−CT imaging and biodistribution studies of ^{111}In-neunpa−trastuzumab were performed using female NOD.Cg-Prkdc^{scid} Il2rg^{tm1Wjl}/SzJ mice bearing SKOV-3 xenografts, and it was found that ^{111}In-neunpa−trastuzumab successfully identified the tumor from surrounding tissues and other organs. Compared to the gold-standard ^{111}In−CHX-A″−DTPA−trastuzumab, our immunoconjugate showed slightly lower tumor uptake, which decreased over time and a lower tumor-to-blood ratio after 5 days post-injection, although high-quality SPECT−CT images were obtained. A different pharmacokinetic behavior of both immunoconjugates can be the result of different charges on the immunoconjugates. Thermodynamic stability experiments support these findings because p-NO_2−Bn−H_4neunpa was found to bind strongly to large, highly charged metal ions such as In^{3+}, La^{3+}, and Bi^{3+}. Indeed, these results suggest H_4neunpa as a strong Bi(III) chelator and, considering the higher 3.6 unit pM value with respect to its In(III) complex, it could be of interest for Bi(III) isotopes (^{212}Bi and ^{213}Bi) in targeted α therapy (TAT). These encouraging results suggest H_4neunpa and its immunoconjugate have promise for studies with other radiometals and targeting vectors. These experiments are currently underway.

EXPERIMENTAL SECTION

Materials and Methods. All solvents and reagents were from commercial sources (Sigma-Aldrich, TCI) and were used as received unless otherwise noted. p-NH_2−Bn−CHX-A″−DTPA and p-SCN−Bn−CHX-A″−DTPA were purchased from Macrocyclics (Dallas, TX) and used as received. Human serum was purchased frozen from Sigma-Aldrich. ^{1}H and ^{13}C NMR spectra were recorded at room temperature on a Bruker AV400 instrument; the NMR spectra are expressed on the δ (ppm) scale and are referenced to the residual solvent signal of the deuterated solvent. All spectra were recorded with sweep widths of 0−14 ppm or −20−220 ppm for ^{1}H and ^{13}C NMR, respectively, and deviations in the presented spectra are magnifications for visualization purpose only. Assignments of the peaks in the NMR spectra are approximate. Mass spectrometry was performed on a Waters ZQ spectrometer equipped with an electrospray source. The HPLC system used for purification of ligands and precursors consisted of a Waters

DOI: 10.1021/acs.bioconjchem.7b00311
Bioconjugate Chem. 2017, 28, 2145−2159

600 controller equipped with a Waters 2487 dual λ absorbance detector connected to a Phenomenex synergi hydro-RP 80 Å 250 mm × 21.1 mm semipreparative column. Analysis of ^{111}In and ^{177}Lu radiolabeled chelate complexes was carried out using a Phenomenex Synergi 4 μ Hydro-RP 80 Å analytical column (250 mm × 4.60 mm 4 μm) using an Agilent HPLC system equipped with a model 1200 quaternary pump, a model 1200 UV absorbance detector (set at 250 nm), and a Raytest Gabi Star NaI(Tl) detector. The radiochemical purity and specific activity of the final ^{111}In radioimmunoconjugates was determined by using a size-exclusion chromatography (SEC) column (Phenomenex, BioSep-SEC-s-3000) on an Agilent HPLC system equipped with a model 1200 quaternary pump, a model 1200 UV absorbance detector (set at 280 nm), and a Bioscan (Washington, DC) NaI scintillation detector (the radiodetector was connected to a Bioscan B-FC-1000 flow-count system, and the output from the Bioscan flow-count system was fed into an Agilent 35900E interface, which converted the analog signal to a digital signal). Instant thin-layer chromatography (TLC) paper strips impregnated with silica gel (iTLC-SG, Varian) were used to analyze crude ^{111}In immunoconjugate-labeling reactions and complex stability and counted on either a BioScan System 200 imaging scanner equipped with a BioScan Autochanger 1000 or on a Raytest miniGita with β GMC detector radio-TLC plate reader using TLC control Mini Ginastar software. PD-10 desalting columns (Sephadex G-25 M, 50 kDa, GE Healthcare) and centrifugal filter units with a 50 kDa molecular weight cutoff (Ultracel-50: regenerated cellulose, Amicon Ultra 4 Centrifugal Filtration Units, Millipore Corporation) were used for purification and concentration of antibody conjugates.

$^{111}InCl_3$ was cyclotron-produced and provided by Nordion as a ~0.05 M HCl solution. $^{117}LuCl_3$ was purchased from PerkinElmer and provided as a solution in dilute HCl.

N,N-(2-Nitrobenzensulfonamide)-1,2-triaminodiethane, ***1***. Diethylenetriamine (4.19 mL, 38.8 mmol) was dissolved in THF (240 mL) and cooled to 0 °C. Sodium carbonate Na_2CO_3 (9.04 g, 2.2 equiv) was added, followed by the slow addition of 2-nitrobenzensulfonyl chloride (18.9 g, 85.3 mmol, 2.2 equiv), causing the reaction mixture to turn pale yellow. The reaction mixture was stirred overnight at room temperature. The off-white mixture was filtered to remove sodium carbonate, and the filtrate was rotary evaporated to dryness. The crude product was purified by silica chromatography (CombiFlash R_f automated column system 220 g HP silica; solid (pause) preparation; A, hexanes; B, ethyl acetate; C, methanol; 100% A to 100% B gradient followed by 100% C) to yield the product **1** as a yellow-orange solid (88%, 16.15 g). ^{1}H NMR (400 MHz, acetone-d_6, 25 °C): 8.13−8.11 (m, 2H), 7.94−7.89 (m, 6H), 3.11 (t, J = 7.32 Hz, 4H), 2.67 (t, J = 5.80 Hz, 4H). ^{13}C NMR (101 MHz, acetone-d_6, 25 °C): 134.0, 132.7, 130.7, 125.0, 47.7, and 43.1. HR-ESI-MS: $[C_{16}H_{19}N_5O_8S_2 + H]^+$ calcd., 474.0753; $[M + H]^+$ found, 474.0749.

N,N-(((4-Nitrophenyl)azanediyl)bis(ethane-2,1-diyl))bis(2-nitrobenzenesulfonamide), ***2***. To a solution of **1** (16.15 g, 34.1 mmol) in DMF (60 mL) was added K_2CO_3 (6.13 g, 44.3 mmol, 1.3 equiv) and 4-(2-bromoethyl)nitrobenzene (10.20 g, 44.3 mmol, 1.3 equiv). After the reaction mixture was stirred for 3 days at 40 °C, the bright yellow solution was cooled to room temperature, and the excess K_2CO_3 was removed by centrifugation. After the solution was dried in vacuo, the crude dark red product was purified by silica chromatography (Combi Flash R_f automated column system; 80 g of HP silica; solid (pause) preparation; A, hexane; B, ethyl acetate; 100% A to 100% B gradient) to yield product **2** as an orange fluffy solid (64.0%, 13.59 g). ^{1}H NMR (400 MHz, $CDCl_3$, 25 °C): 8.11−8.09 (d, J = 8.58 Hz, 2H), 8.08−8.06 (m, 2H), 7.84−7.81 (m, 2H), 7.76−7.73 (m, 4H), 7.32−7.30 (d, d = 8.58 Hz, 2H), 5.68 (s, 2H, NH), 3.07−3.05 (t, d = 5.63, 4H), 2.86−2.82 (t, J = 6.88, 2H), 2.74−2.72 (m, 2H), 2.70−2.67 (t, J = 6.62 Hz, 4H). ^{13}C NMR (101 MHz, $CDCl_3$, 25 °C): 158.0, 157.6, 147.5, 146.8, 129.6, 129.5, 124.0, 117.3, 114.4, 55.0, 52.5, 37.6, 33.5. HR-ESI-MS: $[C_{24}H_{26}N_6O_{10}S_2 + H]^+$, calcd., 623.1230; $[M + H]^+$ found, 623.1237.

Dimethyl-6,6-(((((4-nitrophenethyl)azanediyl)bis(ethane-2,1-diyl))bis(((2-nitrophenyl)sulfonyl)azanediyl))bis-(methylene))dipicolinate, ***3***. To a solution of **2** (13.59 g, 21.8 mmol) in dry DMF (80 mL) was added methyl-6-bromomethyl picolinate (11.55 g, 50.2 mmol, 2.3 equiv) and sodium carbonate (5.32 g, 50.2 mmol, 2.3 equiv). The bright orange reaction mixture was stirred at 60 °C overnight, filtered to remove excess sodium carbonate, and concentrated in vacuo. The crude product was purified by silica chromatography (CombiFlash R_f automated column system; 2 × 80 g of silica; solid (pause) preparation; A, hexane; B, ethyl acetate; 100% A to 100% B gradient) to yield product **3** as an orange/brown oil (70%, 14 g). ^{1}H NMR (400 MHz, $CDCl_3$, 25 °C): 8.02−8.00 (m, 4H), 7.96 (d, J = 7.7 Hz, 2H), 7.78 (t, J = 7.8 Hz, 2H), 7.67−7.60 (m, 6H), 7.54 (d, J = 7.8 Hz, 2H), 7.18 (d, J = 8.4 Hz, 2H), 4.67 (s, 4H), 3.89 (s, 6H), 3.29 (t, J = 6.8 Hz, 4H), 2.58−2.51 (m, 8H). ^{13}C NMR (101 MHz, $CDCl_3$, 25 °C): 165.3, 157.0, 148.1, 147.6, 146.4, 138.1, 132.1, 129.7, 126.0, 125.9, 124.4, 124.4, 123.5, 55.3, 53.9, 52.9, 52.7, 46.9, and 33.4. HR-ESI-MS: $[C_{40}H_{40}N_8O_{14}S_2 + H]^+$ calcd., 921.2184; $[M + H]^+$ found, 921.2184.

Dimethyl-6,6-(((((4-nitrophenethyl)azanediyl)bis(ethane-2,1-diyl)bis(azanediyl))bis(methylene))dipicolinate, ***4***. To a solution of **3** (7.48 g, 8.1 mmol) in dry THF (100 mL) was added thiophenol (1.91 mL, 18.7 mmol, 2.3 equiv) and potassium carbonate (3.71 g, 26.8 mmol, 3.3 equiv). The reaction mixture was stirred at 50 °C for 72 h, changing color to light orange. The excess salts were removed by centrifugation (5 min, 4000 rpm) followed by several washes with DMF. The filtrate was concentrated in vacuo in a (maximum) 50 °C water bath temperature. The resulting crude dark orange oil was purified by neutral alumina chromatography (CombiFlash R_f automated column system; 6 × 40 g of neutral alumina; liquid injection A, dichlormethane; B, methanol; 100% A to 20% B gradient) to yield product **4** as an orange oil (32.4%, 1.45 g). ^{1}H NMR (400 MHz, $CDCl_3$, 25 °C): 8.01 (d, J = 8.6 Hz, 2H), 7.90 (d, J = 7.6 Hz, 2H), 7.73 (t, J = 7.8 Hz, 2 H), 7.45 (d, J = 7.7 Hz, 2H), 7.28 (d, J = 8.6 Hz, 2H), 3.99 (s, 4H), 3.91 (s, 6H), 2.79−2.72 (m, 12H). ^{13}C NMR (101 MHz, $CDCl_3$, 25 °C): 165.6, 158.9, 148.6, 147.4, 164.4, 137.8, 129.7, 126.0, 123.9, 123.7, 55.9, 54.0, 53.0, 52.7, 47.0, 33.3. HR-ESI-MS: $[C_{28}H_{34}N_6O_6 + H]^+$ calcd., 551.2618; $[M + H]^+$ found, 551.2617.

N,N-[(tert-Butoxycarbonyl)methyl-N,N-[6-(methoxycarbonyl)pyridine-2-yl]methyl]-N-(4-nitrophenethyl)-1,2-triaminodiethane, ***5***. To a solution of **4** (1.45 g, 2.6 mmol) in acetonitrile (60 mL) was added *tert*-butylbromoacetate (894 μL, 6.1 mmol, 2.3 equiv) and sodium carbonate (642 mg, 6.1 mmol, 2.3 equiv). The reaction mixture was stirred at 60 °C overnight, filtered to remove excess sodium carbonate, and concentrated in vacuo. The crude product was purified by silica chromatography (CombiFlash R_f automated system; 40 g

DOI: 10.1021/acs.bioconjchem.7b00311
Bioconjugate Chem. 2017, 28, 2145−2159

of HP silica; A, dichloromethane; B, methanol; 100% A to 20% B gradient) to yield product **5** as an orange oil (72%, 1.48 g). ^{1}H NMR (400 MHz, $CDCl_3$, 25 °C): 8.11 (d, J = 8.5 Hz, 2H), 8.03 (d, J = 7.7 Hz, 2H), 7.89 (t, J = 7.7 Hz, 2H), 7.52 (d, J = 7.6 Hz, 2H), 7.43 (d, J = 8.5 Hz, 2H), 4.18 (s, 4H), 3.96 (s, 6H), 3.90 (s, 4H), 3.73 (m, 2H), 3.54 (s, 4H), 3.45 (br s, 4H), 3.24 (m, 2H), 1.38 (s, 18H). ^{13}C NMR (101 MHz, $CDCl_3$, 25 °C): 168.7, 165.1, 156.7, 147.3, 147.3, 143.8, 139.1, 130.1, 127.5, 125.0, 124.0, 83.2, 57.5, 56.0, 54.5, 53.3, 50.4, 48.8, 29.8, 28.0. HR-ESI-MS: $[C_{40}H_{54}N_6O_{10}H]^+$ calcd. 779.3980; $[M + H]^+$ found, 779.3973.

*p-NO_2–Bn–H_4neunpa·2.2 HCl·3.1 H_2O, **6**.* To compound **5** (0.23 g, 0.3 mmol) in THF/H_2O (3 mL, 3:1) was added lithium hydroxide (0.07 g, 3.0 mmol, 10 equiv), and the mixture was stirred for 16 h at room temperature. Solvents were evaporated, and the crude product was purified by semipreparative reverse-phase (RP) HPLC (10 mL/min, gradient A, 0.1% TFA in deionized water; B, acetonitrile; A, 95% to B, 100% for 25 min, t_R= 14.00 min), and the product **6** was obtained as a yellow oil (61%, 0.12 g). ^{1}H NMR (400 MHz, $CDCl_3$, 25 °C): 8.11 (d, J = 8.5 Hz, 2H), 8.03 (d, J = 7.7 Hz, 2H), 7.89 (t, J = 7.7 Hz, 2H), 7.52 (d, J = 7.6 Hz, 2H), 7.43 (d, J = 8.5 Hz, 2H), 4.18 (s, 4H), 3.90 (s, 4H), 3.73 (m, 2H), 3.54 (s, 4H), 3.45 (br s, 4H), 3.24 (m, 2H). ^{13}C NMR (101 MHz, $CDCl_3$, 25 °C): 168.7, 165.1, 156.7, 147.3, 147.3, 143.8, 139.1, 130.1, 127.5, 125.0,124.0, 57.5, 56.0, 54.5, 48.8. HR-ESI-MS: $[C_{30}H_{34}N_6O_{10} + H]^+$ calcd., 639.2415; $[M + H]^+$ found, 639.2415. Elemental analysis: calcd. % for *p*-NO_2–Bn–H_4neunpa·2.2 HCl·3.1 H_2O/C 46.55 N 10.86 H 5.2; found: C 46.72, N 10.64, H 5.37.

*N,N-[(tert-Butoxycarbonyl)methyl-N,N-[6-(methoxycarbonyl)pyridine-2-yl]methyl]-N-(4-aminophenethyl)-1,2-triaminodiethane, **7**.* Compound **5** (0.11 g, 0.1 mmol) was dissolved in glacial acetic acid (3 mL), and Pd/C 10% was added, and the vessel was sealed and purged with H_2 gas and charged with a H_2 balloon and left to stir for 2 h at room temperature. The reaction mixture was then filtered through Celite and concentrated under reduced pressure to yield compound **7**. The aromatic amine was confirmed by a purple ninhydrin staining. The solution was filtered, and the filtrate was concentrated in vacuo. ^{1}H NMR (400 MHz, MeOD, 25 °C): 7.99 (m, 2H), 7.92 (t, J = 7.9 Hz, 2H), 7.62 (d, J = 7.7 Hz, 2H), 6.87 (d, J = 7.9 Hz, 2H), 4.01 (s, 2H), 3.46 (br.4, 2H), 3.13 (m, 4H), 2.79 (m, 4H), 1.41 (s, 18H). ^{13}C NMR (400 MHz, MeOD): 172.3, 166.7, 160.8, 148.3, 139.7, 139.5, 130.4, 128.3, 125.4, 125.2, 116.8, 82.7, 59.4, 56.9, 53.4, 52.3, 50.6, 29.9, 28.4. HR-ESI-MS: $[C_{40}H56N_6O_8 + H]^+$ calcd., 749.4238; $[M + H]^+$ found, 749.4236.

*p-NH_2–Bn–H_4neunpa, **8**.* Compound **6** (0.09 g, 0.13 mmol) was dissolved in THF/H_2O (3 mL, 3:1), and lithium hydroxide (0.03 g, 1.26 mmol, 10 equiv) was added. The reaction mixture was left at room temperature for 24 h. After product formation was confirmed by ESI-MS analysis, the solution was neutralized with 1 M HCl, and solvents were concentrated in vacuo. For purification, semipreparative reverse-phase high-performance liquid chromatography (RP-HPLC; 10 mL/min; gradient A, 0.1% TFA in deionized water; B, acetonitrile; A, 95% to B, 100% for 25 min; t_R= 11.50 min) was used, and product **8** was obtained as a yellow oil (50%, 0.04 g). ^{1}H NMR (400 MHz, MeOD, 25 °C): 8.05–8.04 (d, J = 6.6 Hz, 2H), 7.96–7.94 (d, J = 5.8 Hz, 2H), 7.63–7.61 (d, J = 6.6 Hz, 2H), 7.42–7–40 (d, J = 5.8 Hz, 2H), 7.32 (s, 2H), 4.08 (s, 4H), 3.71 (s, 4H), 3.59 (s, 2H), 3.53 (s, 4H), 3.35 (s, 4H), 3.14 (m, 2H). ^{13}C NMR (400 MHz, MeOD): 173.5, 167.4, 159.0, 148.7, 140.3, 139.1, 131.8, 128.3, 125.6, 124.4, 116.7, 58.7, 56.5, 55.8, 53.1, 50.1, 30.4; ^{13}C-DEPT NMR (400 MHz, MeOD): 140.3↑, 131.5↑, 128.1↑, 125.6↑, 124.2↑, 58.4↓, 56.4↓, 55.5↓, 51.5↓, 49.9↓, 30.2↓. HR-ESI-MS: $[C_{30}H_{37}N_6O_8 + H]^+$ calcd., 609.2673; $[M + H]^+$ found, 609.2671.

*p-SCN–Bn–H_4neunpa, **9**.* Compound **8** (0.04 g, 0.1 mmol) was dissolved in 0.1 M HCl (1 mL) and dichloromethane (1 mL). Thiophosgene (0.05 mL, 0.6 mmol, 10 equiv) was added, and the solution was stirred vigorously at room temperature overnight in the dark. The solvents were concentrated in vacuo and the product purified by semipreparative RP-HPLC (10 mL/min; gradient A, 0.1% TFA in deionized water; B, acetonitrile; A, 95% to B, 100% for 25 min; t_R= 17.00 min) to yield product **9** as an orange oil (59%, 0.02 g). ^{1}H NMR (400 MHz, MeOD, 25 °C): 8.04–8.02 (d, J = 6.7 Hz, 2H), 7.95–7.92 (t, J = 8.2 Hz, 2H), 7.61–7.57 (t, J = 7.5 Hz, 2H), 7.27–7–25 (d, J = 7.5 Hz, 2H), 7.18–7.16 (d, J = 7.5 Hz, 2H), 4.05 (s, 4H), 3.66 (s, 4H), 3.55 (s, 2H), 3.50 (s, 4H), 3.26 (br s, 4H), 3.07 (m, 2H). ^{13}C NMR (400 MHz, MeOD): 173.5, 167.4, 159.0, 148.7, 140.3, 137.5, 131.5, 128.3, 126.9, 125.6, 115.9, 58.7, 56.5, 55.8, 51.9, 50.1, 30.5; ^{13}C-DEPT NMR (400 MHz, MeOD): 140.3↑, 131.4↑, 128.3↑, 126.9↑, 125.6↑, 58.7↓, 56.35↓, 56.5↓, 51.9↓, 50.1↓, 30.5↓. HR-ESI-MS: $[C_{31}H_{35}N_6O_8 + H]^+$ calcd., 651.2237; $[M + H]^+$ found, 651.2239.

Na[La(p-NO_2–Bn–neunpa)]. Compound **6** (10.2 mg, 16.0 mmol) was dissolved in water and lanthanum perchlorate (7.7 mg, 17.6 mmol, 1.1 equiv) was added. The pH was adjusted to 4 using 0.1 M NaOH. The successful La complexation as a white precipitate was confirmed by HR-ESI-MS immediately after the addition of $La(ClO)_4$. After centrifugation, the precipitate was washed with water. ^{1}H NMR (400 MHz, DMSO-d_6, 25 °C): 8.15 (d, 2H), 8.01 (m, 2H), 7.92 (m, 2H), 7.61 (d, J = 7.6 Hz, 2H), 7.50 (d, J = 8.5 Hz, 2H), 4.01 (s, 4H), 3.69 (m, 5H), 3.51 (d, 4H), 3.25 (s, 7H). HSQC (400 MHz, DMSO-d_6, 25 °C) details are in the Supporting Information. HR-ESI-MS: $[_{30}H_{32}N_6O_{10}La]^+$ calcd., 775.1243; $[M + 2H]^+$ found, 775.1236.

Na[Bi(p-NO_2–Bn–neunpa)]. Compound **6** (20.3 mg, 31.8 mmol) was dissolved in water and bismuth trichloride (11.0 mg, 35.0 mmol, 1.1 equiv) was added. The pH was adjusted to 4 using 0.1 M NaOH. The successful bicomplexation as a white precipitate was confirmed by HR-ESI-MS immediately after the addition of $BiCl_3$. After centrifugation, the precipitate was washed with water. The bicomplex is not soluble in any solvent; DMSO-d_6 was chosen for NMR analysis. ^{1}H NMR and ^{13}C NMR not measurable due to solubility problems. HR-ESI-MS: $[C_{30}H_{30}N_6O_{10}Bi]^+$ calcd., 843.1827; $[M + 2H]^+$ found, 843.1835.

Na[In(p-NO_2–Bn–neunpa)]. In a 20 mL screw cap vial, compound **6** (12 mg, 0.019 mmol) was dissolved in H_2O/MeOH (2:1, 1.5 mL). In a separate screw cap vial, $[In(ClO_4)_3]\cdot 8H_2O$ (32 mg) was dissolved in distilled water (0.5 mL) to make a stock solution (64 mg/mL). An aliquot (217 μL, 13.8 mg, 0.0249 mmol) of this In(III) stock solution was added to the chelate solution. The pH of the solution was adjusted from pH 1 to pH 5 using 1 N NaOH and 0.1 M HCl. A stir bar was added, and the reaction was heated to 60 °C in a sand bath and stirred for 3 h with the lid on loosely. The mixture was removed from the heat and allowed to cool to room temperature. A white precipitate had formed, and the solution was then centrifuged and washed with distilled water (5 × 1 mL). After drying under high vacuum, the product as a white solid was

DOI: 10.1021/acs.bioconjchem.7b00311
Bioconjugate Chem. 2017, 28, 2145–2159

collected (4 mg, 0.0053 mmol) with an overall yield of 28%. For the results for ^{1}H and COSY NMR (400 MHz, DMSO-d_6) potential multiple isomers in solutions, see Figure S12. HR-ESI-MS: $[^{115}InC_{30}H_{30}N_6O_{10} + H + Na]^+$ calcd., 773.1038; $[M + H + Na]^+$ found, 773.1039.

Bioconjugation of *p*-SCN−Bn−H$_4$neunpa and *p*-SCN−Bn−CHX-A″−DTPA to Trastuzumab. Trastuzumab (Herceptin, Genentech, San Francisco, CA) was purified using size-exclusion columns (PD-10 desalting columns) and centrifugal filter units with a 50 kDa molecular weight cutoff and phosphate-buffered saline (PBS, pH 7.4) to remove α−α-trehalose dehydrate, L-histidine, and polysorbate 20 additives. The purified antibody was brought up in PBS at pH 7.4. For each chelate−antibody conjugation, PBS (905 μL, pH adjusted to 9.0 using 0.1 M Na_2CO_3) and trastuzumab (Genentech, San Francisco, CA) (4 mg, 75 μL in PBS, pH 7.4) was added to a low-protein-binding Eppendorf tube. To the antibody mixture, 5 equiv of *p*-SCN−Bn−H$_4$neunpa or *p*-SCN−Bn−CHX-A″−DTPA was added, respectively, in small portions (5 × 5 μL in DMSO). The reaction mixture was stirred at ambient temperature overnight and subsequently purified by centrifugal filtration. The final bioconjugates were stored in 0.25 M sodium acetate at −20 °C. Final protein concentration was determined by the Bradford assay.

Chelate Number−Radiometric Isotopic Dilution Assay. The number of accessible chelating ligands conjugated per antibody was determined using previously described methods.[36,37] Briefly, a 1 μCi/uL $[^{111}In]InCl_3$ working solution (nonradioactive In^{3+} spiked with ^{111}In) was prepared with a final In^{3+} concentration of 500 μM in ammonium acetate buffer (0.15 M, pH 6). In duplicate, for each chelate−antibody conjugate, 50 μg of bioconjugate (30 μL) was prepared into separate 1.5 mL Eppendorf tubes. Aliquots of 20, 25, and 30 μL of the $[^{111}In]InCl_3$ working solution were added to the two chelate−antibody samples. Positive controls containing 50 μg of bioconjugate and 25 μL of buffered $^{111}InCl_3$ only (no nonradioactive In^{3+} added) were prepared in duplicate. Negative controls containing 30 μL of PBS, and 25 μL of $[^{111}In]InCl_3$ working solution were prepared in duplicate. Samples were allowed to incubate at room temperature overnight, after which time EDTA (50 mM, pH 5) was added at 1/9 of the reaction volume to scavenge any unspecifically bound In^{3+} and incubated for 15 min. Each reaction mixture was spotted onto instant thin-layer chromatography (TLC)−silica gel (SG) plates and developed using EDTA (50 mM, pH 5) as the mobile phase. Radioactivity on the plate was measured using a radio-TLC plate reader, and the number of chelates attached per antibody was calculated using eq 1:

$$\text{nmol chelate} = \frac{\text{no. counts at baseline } (R_f < 0.2)}{\text{total no. counts}} \times \text{nmol in } ^{3+} \quad (1)$$

^{111}In−Chelate Radiolabeling Studies. The ligand *p*-NO$_2$−Bn−H$_4$neunpa, or gold standard *p*-NH$_2$−Bn−CHX-A″−DTPA, was made up as a stock solution (1 mg/mL, ∼10^{-3} M) in deionized water. From this stock solution, serial dilutions were prepared to final ligand concentrations of 10^{-4}−10^{-9} M. A 100 μL aliquot of each ligand stock (10^{-3} to 10^{-9} M) or water (blank control) was added to screw-cap mass spectrometry vials and diluted with sodium acetate buffer (pH 4, 10 mM, 880 μL). An aliquot of diluted ^{111}In stock (20 μL, ∼200 μCi) was added to each vial and allowed to radiolabel at ambient temperature for 10 min, and it was then analyzed by RP-HPLC to confirm radiolabeling and calculate yields. For human serum stability studies, undiluted $^{111}InCl_3$ stock (∼20 μL, 5 mCi) was added to the reaction vial containing 10^{-4} M ligand in sodium acetate buffer. Areas under the peaks observed in the HPLC radio-trace were integrated to determine radiolabeling yields. Elution conditions used for RP-HPLC analysis were gradient: A, 0.1% trifluoroacetic acid (TFA) in water; B, acetonitrile; 0 to 100% B linear gradient 20 min, 1 mL/min. $[^{111}In(p\text{-}NO_2\text{−}Bn\text{−}neunpa)]^-$ (t_R = 12.9 min), $[^{111}In(p\text{-}NH_2\text{−}Bn\text{−}CHX\text{-}A''\text{−}DTPA)]^{2-}$ (t_R = 8.0 min (minor product); 8.6 min (major product)) "$^{111}In^{3+}$" (t_R = 5.3 min).

Partition Coefficients. ^{111}In-labeled complex (30 μL, 20 μCi) was diluted with phosphate buffered saline (pH 7.4, 470 μL) and added to 1-octanol (500 μL) in a 1.5 mL Eppendorf tube. Samples were vortexed for 60 s and subsequently centrifuged to separate phases (3000 rpm, 5 min). Aliquots (490 μL) of the aqueous and organic phases were diluted in a standard volume (20 mL) of water or acetonitrile, respectively, for measurement in an N-type Coaxial HPGe gamma spectrometer from Canberra fitted with a 0.5 mm beryllium window and calibrated (energy and efficiency) with a 20 mL ^{152}Eu and ^{133}Ba source. The samples were counted for a minimum of 5 min with a dead time of less than 5%. The amount of ^{111}In complex (Bq) in each fraction was quantified using the 171 and 245 keV γ lines of ^{111}In.

^{111}In-neunpa/CHX-A″−DTPA−Trastuzumab Radiolabeling for in Vivo Studies. Aliquots of H$_4$neunpa/CHX-A″−DTPA−trastuzumab (650 μg) were diluted with ammonium acetate buffer (0.15 M, pH 6), such that the final volume of the reaction was 1 mL, and then $^{111}InCl_3$ (∼20 mCi) was added. The mixtures were allowed to react at ambient temperature for 40 min and was then analyzed via iTLC-SG using 50 mM EDTA (pH 5) as eluent; ^{111}In-labeled antibody remained at the baseline, while $^{111}In^{3+}$ ions complexed as ^{111}In−EDTA and eluted with the solvent front. Radiolabeled immunoconjugates were then purified by PD-10 SEC columns and centrifugal filtration (50 000 cutoff). The radiochemical purity of the final radiolabeled bioconjugates was determined using SEC−HPLC (using an isocratic gradient of 0.1 M sodium phosphate monobasic dehydrate, 0.1 M sodium phosphate dibasic dodecahydrate, 0.1 M sodium azide, and 0.15 M sodium chloride [pH 6.2−7.0]); the specific activity was calculated by injecting a known activity, and integrating areas under the peaks of the UV chromatogram measured against a standard curve.

In Vitro Human Serum Stability Data. The procedures of the serum competition studies followed closely those previously published.[8,10] The compound $[^{111}In(p\text{-}NO_2\text{−}Bn\text{−}neunpa)]^-$, $[^{111}In(p\text{-}NH_2\text{−}Bn\text{−}CHX\text{-}A''\text{−}DTPA)]^{2-}$, or blank control "$^{111}In^{3+}$" was prepared using the radiolabeling protocol as described above. In triplicate for the ^{111}In complex, solutions were prepared in vials containing 330 μL of ^{111}In complex (∼1.6 mCi), 1000 μL of room-temperature human serum, and 670 μL of PBS (pH 7.4) and incubated at 37 °C. At time points of 1 h and 1 and 5 days, 400, 400, and 800 μL aliquots of the human serum competition mixture were removed from each vial, respectively, diluted to a total volume of 2.5 mL with PBS, and counted in a Capintec CRC-55tR dose calibrator; this value is recorded as "full activity" to be loaded onto the PD-10 column. The 2.5 mL of reaction mixture was loaded onto a preconditioned PD-10 column, and the empty vial was counted again in the dose calibrator; this value was recorded as "residual

DOI: 10.1021/acs.bioconjchem.7b00311
Bioconjugate Chem. 2017, 28, 2145−2159

activity" left in the vial. The loaded effluent was collected in a waste container, and then the PD-10 column was eluted with 3.5 mL of PBS and collected into a separate vial. The eluent that contained ^{111}In bound and associated with serum proteins (size exclusion for MW < 5000 Da) was counted in the dose calibrator and then compared to the total activity that was loaded onto the PD-10 column to obtain the percentage of ^{111}In that was bound to serum proteins and, therefore, no longer chelate-bound by the relationship of 1 − (eluted activity/(full activity−residual activity) × 100. For serum stability of the radioimmunoconjugates, ^{111}In-neunpa−trastuzumab was first prepared as described above by incubating H_4neunpa−trastuzumab (200 μg) and $^{111}InCl_3$ (∼1 mCi) in NH_4OAc (0.15 M, pH 6) for 20 min at an ambient temperature. After confirmation of a radiolabeling yield >95% via iTLC-SG in 50 mM EDTA (pH 5), in triplicate, ^{111}In-neunpa−trastuzumab (330 μL, ∼320 μCi) was incubated with human serum (330 μL), and the mixture was left at 37 °C for 168 h (7 days). At time points of 0, 1, 24, 48, 120, and 168 h, aliquots (3−5 μL) of the competition mixture was spotted on iTLC-SG plates and developed in 50 mM EDTA (pH 5) as described above.

Cell Culture. The human ovarian adenocarcinoma HER2-positive SKOV-3 cells were cultured at 37 °C with 5% CO_2 in Dulbecco's modified Eagle medium (DMEM, LifeTechnologies, Rockford, IL) containing 2 mM glutamine and supplemented with 10% fetal bovine serum (Sigma-Aldrich, Oakville, ON) and 100 U/mL of penicillin−streptomycin (LifeTechnologies).

In Vitro Immunoreactivity Assay. The immunoreactive fractions of ^{111}In-neunpa−trastuzumab and ^{111}In−CHX-A″−DTPA−trastuzumab were determined according to the Lindmo cell-binding method[38] using SKOV-3 cells[37,39] as previously described. Briefly, cells were suspended at 0.23 to 2.3 × 10^6 cells/mL in PBS (pH 7.4). For each tested antibody, 50 μL (from a solution of 0.45 μg of each radioimmunoconjugate diluted in 5 mL of 1% PBS-BSA) was added to each cell concentration tube in duplicate. The radiolabeled immunoconjugates were incubated for 1 h at 37 °C and under gentle agitation. Cells were then pelleted and washed twice with PBS. Each cell-bound activity for the different cell conditions was determined by measuring the ^{111}In amount of activity within the cell pellets using the Wallac WIZARD2 gamma counter with background and decay correction. The bound fraction was determined as a percentage of total added activity according to control samples. Immunoreactive fractions were estimated for conditions representing infinite antigen excess by linear regression analysis of a plot of total/bound activity against 1/[cell concentration]. Results of >80% were considered suitable for in vivo imaging.

SKOV-3 Xenograft Mouse Models. All experiments were conducted in accordance with the guidelines established by the Canadian Council on Animal Care and approved by the Animal Ethics Committee of the University of British Columbia (protocol no. A16-0104). Female NOD.Cg-Prkdc^{scid} Il2rg^{tm1Wjl}/SzJ mice (4 months old) obtained from an in-house breeding colony were subcutaneously injected with 8 × 10^6 SKOV-3 cells in matrigel (BD Bioscience) on the left flank.

[^{111}In(*p*-NO_2−Bn−neunpa)]$^-$ and [^{111}In(*p*-NH_2−Bn−CHX-A″−DTPA)]$^{2-}$ in Vivo Biodistribution. [^{111}In(*p*-NO_2−Bn−neunpa)]$^-$ and [^{111}In(*p*-NH_2−Bn−CHX-A″−DTPA)]$^{2-}$ were prepared according to the radiolabeling protocol above using 10^{-4} M ligand and ∼148 MBq (∼4 mCi) of $^{111}InCl_3$ in sodium acetate buffer (10 mM, pH 4). Radiolabeling yields >99% were confirmed by RP-HPLC. Each radiolabeled tracer was diluted with PBS (pH 7.4) to a concentration of 10 MBq/mL (370 μCi/mL). Each mouse was intravenously injected through the tail vein with ∼1 MBq (100 μL) of the ^{111}In complex and then sacrificed by inhalation of isoflurane followed by CO_2 at 15 min or 1, 4, or 24 h after injection (n = 4 at each time point). Blood was withdrawn by cardiac puncture and tissues of interest including fat, uterus, ovaries, intestine, spleen, liver, pancreas, stomach, adrenal glands, kidney, lungs, heart, muscle, bone (tibia), brain, and tail were harvested, washed in PBS, dried, and weighed. Activity of each sample was measured by a calibrated γ counter (PerkinElmer, Wizard 2 2480) with decay correction. The activity uptake was expressed as a percentage of the injected dose per gram of tissue (% ID/g).

^{111}In-neunpa/CHX-A″−DTPA−Trastuzumab SPECT−CT Imaging and Biodistribution Studies. Mice with SKOV-3 ovarian cancer xenografts were administered with ∼37 MBq (∼1 mCi) of ^{111}In-neunpa−trastuzumab (1.03 MBq/μg [28.0 μCi/μg]) or ^{111}In−CHX-A″−DTPA−trastuzumab (0.77 MBq/μg [20.8 μCi/μg]) in ∼30 μL of PBS (pH 7.4) via tail-vein injection. For each radioimmunoconjugate, mice were imaged (n = 2) at 1, 3, or 5 days after injection. Image acquisition and reconstruction was performed using the U-SPECT-II−CT (MILabs, Utrecht, The Netherlands). Approximately 5 min prior to SPECT−CT image acquisition, mice were anesthetized via inhalation of 2% isoflurane−oxygen gas mixture and placed on the scanner bed. Anesthesia was maintained during imaging as well as body temperature via a heating pad. A 5 min baseline CT scan was obtained for localization with a voltage setting at 60 kV and current at 615 μA followed by a static emission scan using an ultrahigh-resolution multipinhole rat−mouse (1 mm pinhole size) collimator. Data were acquired in list mode, reconstructed using the U-SPECT II software, and co-registered for alignment. SPECT images were reconstructed using maximum-likelihood expectation maximization (3 iterations), pixel-based ordered subset expectation maximization (16 subsets), and a postprocessing filter (Gaussian blurring) of 0.5 mm centered at photopeaks 171 and 245 keV with a 20% window width. Imaging data sets were decayed, corrected to injection time, and converted to DICOM data for visualization in the Inveon Research Workplace (Siemens Medical Solutions USA, Inc.). Because no calibration factor was used for attenuation, and scatter correction was performed on the images; they were used only for qualitative comparison between the two tracers and are presented using a min−max scale bar of counts corrected for decay. For the biodistribution studies, mice were sacrificed by the inhalation of isoflurane followed by CO_2 (n = 4 at each time point), blood was withdrawn by cardiac puncture, and tissues were collected and processed as described above. Tissues collected include all those listed above in addition to tumor tissue.

Solution Thermodynamics. Protonation constants and metal stability constants were calculated from potentiometric titrations using a Metrohm Titrando 809 equipped with a Ross combined electrode and a Metrohm Dosino 800. The titration apparatus consisted of a 20 mL and 25 °C thermostated glass cell and an inlet−outlet tube for nitrogen gas (purified through a 10% NaOH solution) to exclude any CO_2 prior and during the course of the titration. The electrode was calibrated daily in hydrogen-ion concentrations using a standard HCl as described

DOI: 10.1021/acs.bioconjchem.7b00311
Bioconjugate Chem. 2017, 28, 2145−2159

before[13] to obtain the calibration parameters E_0 and pKw. Solutions were titrated with carbonate-free NaOH (0.157 M) that was standardized against freshly recrystallized potassium hydrogen phthalate. Protonation equilibria of the ligand were studied by titrations of a solution containing H_4neunpa (7.18×10^{-4} M at 25 °C and 0.16 M NaCl ionic strength) using a combined potentiometric−spectrophotometric procedure.[16,17] Spectra were recorded in the 200−450 nm spectral range with a 0.2 cm path length fiber optic on a Varian Cary 60 UV−vis spectrophotometer. In the study of complex formation equilibria, the ligand−metal solutions were prepared by adding the atomic absorption (AA) standard metal ion solutions to a H_4neunpa solution of known concentration in the 1:1 metal-to-ligand molar ratio. The exact amount of acid present in the lanthanum, bismuth, and indium standards was determined by Gran's method[40] by titrating equimolar solutions of either La(III), Bi(III), or In(III) and Na_2H_2−EDTA. Ligand and metal concentrations were in the range of 0.7−1.0 mM. Each titration consisted of 100−150 equilibrium points in the pH range 1.8−11.5, and equilibration times for titrations were 2 min for pK_a titrations and up to 15 min for metal complex titrations. At least two replicate titrations were performed for each individual system. Potentiometric data were processed using the Hyperquad2013 software,[41] while the obtained spectrophotometric data were processed with the HypSpec.[41] Proton dissociation constants corresponding to hydrolysis of La(III), Bi(III), and In(III) aqueous ions and the indium−chloride stability constants included in the calculations were taken from Baes and Mesmer.[42] The overall equilibrium (formation) constants, log β, are referred to the overall equilibria: pM + qH + rL = MpHpLr (the charges are omitted), where p might also be 0 in the case of protonation equilibria and q may be negative. Stepwise equilibrium constants (log K) correspond to the difference in log units between the overall constants of sequentially protonated (or hydroxide) species. The pM values for metal complexes were calculated by using the Hyss software[43] from the set of stability constants for each system at pH 7.4 with [L] = 1.0×10^{-5} M and [M] = 1.0×10^{-6} M.

■ ASSOCIATED CONTENT

Supporting Information

The Supporting Information is available free of charge on the ACS Publications website at DOI: 10.1021/acs.bioconjchem.7b00311.

Figures showing NMR spectra, UV spectroscopic titration, speciation plots and diagrams, RP-HPLC radiochromatograms, iTLC-SG radiotraces, and COSY NMR spectra. A table showing biodistribution data. (PDF)

A 3D video of ^{111}In−CHX-A″−DTPA−trastuzumab on day 1. (MPG)

A 3D video of ^{111}In−CHX-A″−DTPA−trastuzumab on day 3. (MPG)

A 3D video of ^{111}In−CHX-A″−DTPA−trastuzumab on day 5. (MPG)

A 3D video of ^{111}In-neunpa−trastuzumab on day 1. (MPG)

A 3D video of ^{111}In-neunpa−trastuzumab on day 3. (MPG)

A 3D video of ^{111}In-neunpa−trastuzumab on day 5. (MPG)

■ AUTHOR INFORMATION

Corresponding Author

*E-mail: orvig@chem.ubc.ca.

ORCID

Nadine Colpo: 0000-0001-9253-6539

Chris Orvig: 0000-0002-2830-5493

Notes

The authors declare no competing financial interest.

■ ACKNOWLEDGMENTS

Funding for this work was provided by the Canadian Institutes for Health Research (CIHR) and the Natural Sciences and Engineering Research Council (NSERC) of Canada as a Collaborative Health Research Project (CHRP). We acknowledge Nordion (Canada) for their in-kind contribution of $^{111}InCl_3$. TRIUMF receives funding via a contribution agreement with the National Research Council of Canada. We would also like to thank Victoria Braun for assisting with logP measurements and Annabell Martin for synthesis of intermediates.

■ ABBREVIATIONS

SPECT, single photon emission computed tomography; BFC, bifunctional chelator; DOTA, 1,4,7,10-tetraazacyclododecane-1,4,7,10-tetraacetic acid; DTPA, 2-[bis[2-[bis(carboxymethyl)-amino]ethyl]amino]acetic acid; CHX, cyclohexyl; CN, coordination number; HER2/neu, human epidermal growth factor receptor 2; mAb, monoclonal antibody; CT, computed tomography

■ REFERENCES

(1) Holland, J. P., Williamson, M. J., and Lewis, J. S. (2010) Unconventional Nuclides for Radiopharmaceuticals. *Mol. Imaging 9*, 1−20.

(2) Price, E. W., and Orvig, C. (2014) Matching chelators to radiometals for radiopharmaceuticals. *Chem. Soc. Rev. 43*, 260−290.

(3) Tatsi, A., Maina, T., Cescato, R., Waser, B., Krenning, E. P., de Jong, M., Cordopatis, P., Reubi, J. C., and Nock, B. A. (2014) [DOTA]Somatostatin-14 analogs and their (111)In-radioligands: effects of decreasing ring-size on sst1−5 profile, stability and tumor targeting. *Eur. J. Med. Chem. 73*, 30−37.

(4) Mojtahedi, A., Thamake, S., Tworowska, I., Ranganathan, D., and Delpassand, E. S. (2014) The value of (68)Ga-DOTATATE PET/CT in diagnosis and management of neuroendocrine tumors compared to current FDA approved imaging modalities: a review of literature. *Am. J. Nucl. Med. Mol. Imaging 4*, 426−434.

(5) Price, E. W., Cawthray, J. F., Adam, M. J., and Orvig, C. (2014) Modular syntheses of H(4)octapa and H(2)dedpa, and yttrium coordination chemistry relevant to ^{86}Y/^{90}Y radiopharmaceuticals. *Dalton T 43*, 7176−7190.

(6) Price, E. W., Zeglis, B. M., Cawthray, J. F., Lewis, J. S., Adam, M. J., and Orvig, C. (2014) What a Difference a Carbon Makes: H_4octapa vs H_4C_3octapa, Ligands for In-111 and Lu-177 Radiochemistry. *Inorg. Chem. 53*, 10412−10431.

(7) Price, E. W., Zeglis, B. M., Lewis, J. S., Adam, M. J., and Orvig, C. (2014) H(6)phospa-Trastuzumab: Bifunctional Methylenephosphonate-based Chelator with ^{89}Zr, ^{111}In and ^{177}Lu. *Dalton Trans. 43*, 119−131.

(8) Ramogida, C. F., Cawthray, J. F., Boros, E., Ferreira, C. L., Patrick, B. O., Adam, M. J., and Orvig, C. (2015) H_2CHXdedpa and H_4CHXoctapa—Chiral Acyclic Chelating Ligands for ^{67}/^{68}Ga and ^{111}In Radiopharmaceuticals. *Inorg. Chem. 54*, 2017−2031.

(9) Price, E. W., Zeglis, B. M., Cawthray, J. F., Ramogida, C. F., Ramos, N., Lewis, J. S., Adam, M. J., and Orvig, C. (2013) H4octapa-

DOI: 10.1021/acs.bioconjchem.7b00311
Bioconjugate Chem. 2017, 28, 2145−2159

Trastuzumab: Versatile Acyclic Chelate System for ^{111}In and ^{177}Lu Imaging and Therapy. *J. Am. Chem. Soc. 135*, 12707−12721.
(10) Price, E. W., Cawthray, J. F., Bailey, G. A., Ferreira, C. L., Boros, E., Adam, M. J., and Orvig, C. (2012) H_4octapa: An Acyclic Chelator for ^{111}In Radiopharmaceuticals. *J. Am. Chem. Soc. 134*, 8670−8683.
(11) Shannon, R. D. (1976) Revised effective ionic radii and systematic studies of interatomic distances in halides and chalcogenides. *Acta Crystallogr., Sect. A: Cryst. Phys., Diffr., Theor. Gen. Crystallogr. 32*, 751−767.
(12) Arane, K. (2015) Synthesis and Characterization of H_5decapa and Related Ligand, in *Department of Inorganic Chemistry*; University of British Columbia.
(13) Weekes, D. M., Ramogida, C. F., Jaraquemada-Peláez, M. d. G., Patrick, B. O., Apte, C., Kostelnik, T. I., Cawthray, J. F., Murphy, L., and Orvig, C. (2016) Dipicolinate Complexes of Gallium(III) and Lanthanum(III). *Inorg. Chem. 55*, 12544−12558.
(14) Montavon, G., Le Du, A., Champion, J., Rabung, T., and Morgenstern, A. (2012) DTPA complexation of bismuth in human blood serum. *Dalton Trans. 41*, 8615−8623.
(15) Burai, L., Fabian, I., Kiraly, R., Szilagyi, E., and Brucher, E. (1998) Equilibrium and kinetic studies on the formation of the lanthanide(III) complexes, [Ce(dota)]- and [Yb(dota)]- (H_4dota = 1,4,7,10-tetraazacyclododecane-1,4,7,10-tetraacetic acid). *J. Chem. Soc., Dalton Trans.*, 243−248.
(16) Nurchi, V. M., Crisponi, G., Crespo-Alonso, M., Lachowicz, J. I., Szewczuk, Z., and Cooper, G. J. S. (2013) Complex formation equilibria of CuII and ZnII with triethylenetetramine and its mono- and di-acetyl metabolites. *Dalton Trans. 42*, 6161−6170.
(17) Nurchi, V. M., Lachowicz, J. I., Crisponi, G., Murgia, S., Arca, M., Pintus, A., Gans, P., Niclos-Gutierrez, J., Dominguez-Martin, A., Castineiras, A., Remelli, M., Szewczuk, Z., and Lis, T. (2011) Kojic acid derivatives as powerful chelators for iron(iii) and aluminium(iii). *Dalton Trans. 40*, 5984−5998.
(18) Mato-Iglesias, M., Balogh, E., Platas-Iglesias, C., Toth, E., de Blas, A., and Rodriguez Blas, T. (2006) Pyridine and phosphonate containing ligands for stable lanthanide complexation. An experimental and theoretical study to assess the solution structure. *Dalton Trans.*, 5404−5415.
(19) Kálmán, F. K., Végh, A., Regueiro-Figueroa, M., Tóth, É., Platas-Iglesias, C., and Tircsó, G. (2015) H_4octapa: Highly Stable Complexation of Lanthanide(III) Ions and Copper(II). *Inorg. Chem. 54*, 2345−2356.
(20) Moeller, T., and Thompson, L. (1962) Observations on the rare earths—LXXV (1): The stabilities of diethylenetriaminepentaacetic acid chelates. *J. Inorg. Nucl. Chem. 24*, 499−510.
(21) Standard Reference Data, Smith, R. M., Martell, A. E., and Motekaitis, R. J. (2004) NIST critically selected stability constants of metal complexes database, Standard Reference Data Program, National Institute of Standards and Technology, U.S. Department of Commerce, Gaithersburg, MD..
(22) Csajbók, É., Baranyai, Z., Bányai, I., Brücher, E., Király, R., Müller-Fahrnow, A., Platzek, J., Radüchel, B., and Schäfer, M. (2003) Equilibrium, ^{1}H and ^{13}C NMR Spectroscopy, and X-ray Diffraction Studies on the Complexes Bi(DOTA)- and Bi(DO3A-Bu). *Inorg. Chem. 42*, 2342−2349.
(23) Geraldes, C. F. G. C., Delgado, R., Urbano, A. M., Costa, J., Jasanada, F., and Nepveu, F. (1995) Complexes of Ga^{3+} and In^{3+} with the N,N[double prime]-bis(butylamide) derivative of diethylenetriaminepentaacetic acid: stability constants and nuclear magnetic resonance studies in aqueous solution. *J. Chem. Soc., Dalton Trans.*, 327−335.
(24) Martell, A. E., and Smith, R. M. (1974−1989) *Critical Stability Constants*, Vol. *1*−*6*, Plenum Press: New York.
(25) Lima, L. M. P., Beyler, M., Delgado, R., Platas-Iglesias, C., and Tripier, R. (2015) Investigating the Complexation of the Pb^{2+}/Bi^{3+} Pair with Dipicolinate Cyclen Ligands. *Inorg. Chem. 54*, 7045−7057.
(26) Ramogida, C. F., and Orvig, C. (2013) Tumour targeting with radiometals for diagnosis and therapy. *Chem. Commun. 49*, 4720−4739.
(27) Hosseinimehr, S. J., Orlova, A., and Tolmachev, V. (2010) Preparation and in vitro evaluation of ^{111}In-CHX-A″-DTPA-labeled anti-VEGF monoclonal antibody bevacizumab. *Hum. Antibodies 19*, 107−111.
(28) Massa, S., Vikani, N., Betti, C., Ballet, S., Vanderhaegen, S., Steyaert, J., Descamps, B., Vanhove, C., Bunschoten, A., et al. (2016) Sortase A-mediated site-specific labeling of camelid single-domain antibody-fragments: a versatile strategy for multiple molecular imaging modalities. *Contrast Media Mol. Imaging 11*, 328−339.
(29) Shin, I. S., Lee, S. M., Kim, H. S., Yao, Z., Regino, C., Sato, N., Cheng, K. T., Hassan, R., Campo, M. F., Albone, E. F., et al. (2011) Effect of chelator conjugation level and injection dose on tumor and organ uptake of ^{111}In-labeled MORAb-009, an anti-mesothelin antibody. *Nucl. Med. Biol. 38*, 1119−1127.
(30) Timmermand, O. V., Ulmert, D., Evans-Axelsson, S., Pettersson, K., Bjartell, A., Lilja, H., Strand, S.-E., and Tran, T. A. (2014) Preclinical imaging of kallikrein-related peptidase 2 (hK2) in prostate cancer with a ^{111}In-radiolabelled monoclonal antibody, 11B6. *EJNMMI Research 4*, 51.
(31) Tolmachev, V., Xu, H., Wållberg, H., Ahlgren, S., Hjertman, M., Sjöberg, A., Sandström, M., Abrahmsén, L., Brechbiel, M. W., and Orlova, A. (2008) Evaluation of a Maleimido Derivative of CHX-A″ DTPA for Site-Specific Labeling of Affibody Molecules. *Bioconjugate Chem. 19*, 1579−1587.
(32) Camera, L., Kinuya, S., Garmestani, K., Wu, C., Brechbiel, M. W., Pai, L. H., McMurry, T. J., Gansow, O. A., Pastan, I., Paik, C. H., et al. (1994) Evaluation of the serum stability and in vivo biodistribution of CHX-DTPA and other ligands for yttrium labeling of monoclonal antibodies. *Journal of nuclear medicine: official publication, Society of Nuclear Medicine 35*, 882−889.
(33) Ando, A., Ando, I., Hiraki, T., and Hisada, K. (1989) Relation between the location of elements in the periodic table and various organ-uptake rates. *Nucl. Med. Biol. 16*, 57−80.
(34) Vosjan, M. J., Perk, L. R., Visser, G. W., Budde, M., Jurek, P., Kiefer, G. E., and van Dongen, G. A. (2010) Conjugation and radiolabeling of monoclonal antibodies with zirconium-89 for PET imaging using the bifunctional chelate p-isothiocyanatobenzyl-desferrioxamine. *Nat. Protoc. 5*, 739−743.
(35) Tabrizi, M., Bornstein, G. G., and Suria, H. (2010) Biodistribution mechanisms of therapeutic monoclonal antibodies in health and disease. *AAPS J. 12*, 33−43.
(36) Meares, C. F., McCall, M. J., Reardan, D. T., Goodwin, D. A., Diamanti, C. I., and McTigue, M. (1984) Conjugation of antibodies with bifunctional chelating agents: isothiocyanate and bromoacetamide reagents, methods of analysis, and subsequent addition of metal ions. *Anal. Biochem. 142*, 68−78.
(37) Deri, M. A., Ponnala, S., Kozlowski, P., Burton-Pye, B. P., Cicek, H. T., Hu, C., Lewis, J. S., and Francesconi, L. C. (2015) p-SCN−Bn−HOPO: A Superior Bifunctional Chelator for ^{89}Zr ImmunoPET. *Bioconjugate Chem. 26*, 2579−2591.
(38) Lindmo, T., Boven, E., Cuttitta, F., Fedorko, J., and Bunn, P. A., Jr. (1984) Determination of the immunoreactive fraction of radiolabeled monoclonal antibodies by linear extrapolation to binding at infinite antigen excess. *J. Immunol. Methods 72*, 77−89.
(39) Rousseau, J., Zhang, Z., Dias, G. M., Zhang, C., Colpo, N., Bénard, F., and Lin, K.-S. (2017) Design, synthesis and evaluation of novel bifunctional tetrahydroxamate chelators for PET imaging of 89Zr-labeled antibodies. *Bioorg. Med. Chem. Lett. 27*, 708−712.
(40) Gran, G. (1952) Determination of the equivalence point in potentiometric titrations. Part II. *Analyst 77*, 661−671.
(41) Gans, P., Sabatini, A., and Vacca, A. (1996) Investigation of equilibria in solution. Determination of equilibrium constants with the HYPERQUAD suite of programs. *Talanta 43*, 1739−1753.
(42) Baes, C. F. J., and Mesmer, R. E. (1976) *The Hydrolysis of Cations*; Wiley, New York.
(43) Alderighi, L., Gans, P., Ienco, A., Peters, D., Sabatini, A., and Vacca, A. (1999) Hyperquad simulation and speciation (HySS): a utility program for the investigation of equilibria involving soluble and partially soluble species. *Coord. Chem. Rev. 184*, 311−318.

DOI: 10.1021/acs.bioconjchem.7b00311
Bioconjugate Chem. 2017, 28, 2145−2159